Heterodyne dispersive cavity ring-down spectroscopy exploiting eigenmode frequencies for high-fidelity measurements

Agata Cygan, Szymon Wójtewicz, Hubert Jóźwiak, Grzegorz Kowzan, Nikodem Stolarczyk, Katarzyna Bielska, Piotr Wcisło, Roman Ciuryło, Daniel Lisak

Institute of Physics, Faculty of Physics, Astronomy and Informatics, Nicolaus Copernicus University in Toruń, Grudziadzka 5, 87-100 Torun, Poland

Measuring low light absorption with combined uncertainty < 1‰ is crucial in a wide range of applications. Popular cavity ring-down spectroscopy can provide ultra-high precision, below 0.01‰, but its accuracy is strongly dependent on the measurement capabilities of the detection system and typically is about 10‰. Here, we exploit the optical frequency information carried by the ring-down cavity electromagnetic field, not explored in conventional CRDS, for high-fidelity spectroscopy. Instead of measuring only the decaying light intensity, we perform heterodyne detection of ring-downs followed by Fourier analysis to provide exact frequencies of optical cavity modes and a dispersive spectrum of a gas sample from them. This approach is insensitive to inaccuracies in light intensity measurements and eliminates the problem of detector band nonlinearity, the main cause of measurement error in traditional CRDS. Using the CO and HD line intensities as examples, we demonstrate the sub-‰ accuracy of our method, confirmed by the best *ab initio* results, and the long-term repeatability of our dispersion measurements at 10^{-4} level. Such results have not been achieved in optical spectroscopy before. The high accuracy of the presented method indicates its potential in atmospheric studies, isotope ratio metrology, thermometry, and the establishment of primary gas standards.

The challenge of measuring the shape and intensity of spectral lines with a relative accuracy of 10^{-3} and better is highlighted in numerous scientific, industrial, and metrological applications using sensitive optical spectroscopy. Regarding the effect of global warming, changes in the Earth's climate are expected to impact the capacity of natural repositories of anthropogenic greenhouse gases (GHG), which will generate a feedback response to climate change[1]. To predict the evolution of these changes, the location of regional sources and sinks of GHG is essential. Spectroscopic retrieval models must exhibit sensitivity to changes in their concentration at the permille level, necessitating a laboratory spectra accuracy of at least an equivalent magnitude[2]. Any systematic errors are of great concern because they introduce regional bias that imitates sources and sinks of GHG. Particular attention is also required in measurements of the stable isotope ratio, as repeatability is compromised over time due to the aging of reference materials[3]. A promising approach involves the spectroscopic measurement of the absolute isotope ratio from the ratio of the line intensities of these isotopes. This method has recently demonstrated[4] a relative combined measurement uncertainty at the sub-‰ level, showing good agreement with the results obtained from other methods. However, to measure line intensities with such high accuracy, careful calibration of the light intensity detection system is necessary[5]. Accurate measurements of the line intensity ratios are also the basis for the new concept of optical primary thermometry[6]. With the current standard of using first principles to define the units of temperature, pressure, and number density[7], optical methods offer promising prospects for realizing new primary gas standards[8]. As molecules interact with electromagnetic radiation, the accurate measurements of the refractive index enable the determination of gas thermodynamic parameters. Cavity-based nitrogen refractometry with a relative precision of 10^{-6} holds the greatest potential for realizing an optical primary pressure standard[9,10] to date. On the other hand, individual spectral lines, shaped by molecular interactions, provide molecular selectivity for optical gas standards. Progress in the mutual development of line-shape theory and spectroscopic methods[11] motivates continuous improvement in *ab initio* accuracies of spectral line intensities[12,13], which opens new possibilities for developing gas mixture and pressure standards related to accurate measurement of line intensity.

Many of these applications use cavity ring-down spectroscopy[14] (CRDS) to quantitatively measure trace and weakly absorbing species in the gas phase. Traditional CRDS systems, widely used due to their simplicity, reliability, and calibration-free nature, with inherently high sensitivity and spectral resolution, have been improved with laser and cavity stabilization technologies[15,16], and optical frequency combs providing accurate absolute frequency axes[17]. Although the best obtained relative precision exceeds 10^{-5}, the determined line intensities can differ by up to several percent between spectrometers due to the limited ability to measure the undistorted ring-down signals[5,18]. As long as the light is turned off quickly enough, the main factors that limit the accuracy of CRDS are

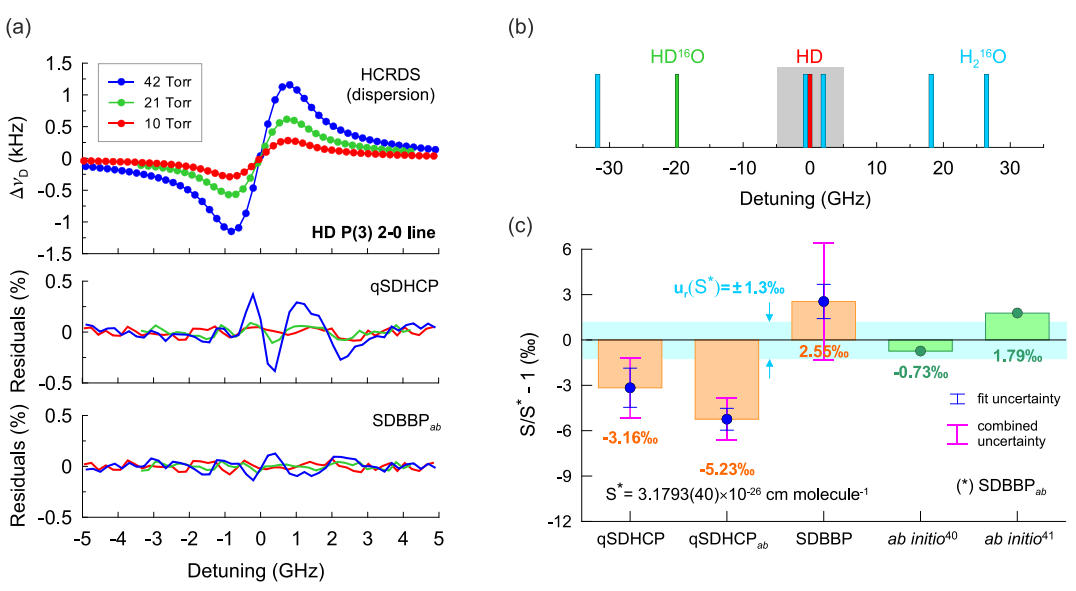

Figure 3 | Permille-level accuracy spectroscopy of the molecular hydrogen line shape. a, The dispersive HCRDS spectrum of the P(3) 2-0 line of HD ($\tilde{\nu}_0$ = 6798.7679 cm^{-1}) measured at temperature 296 K at pressures ranging from 10 to 42 Torr. The residuals below correspond to the difference between the experimental model and the fitted line-shape model. In fits qSDHCP and SDBBP$_{ab}$ were used. The subscript *ab* indicates that line-shape parameters such as collisional width and shift, Dicke narrowing and speed dependence of collisional width and shift were set to the *ab initio* values. Each spectrum is an average of 5000-15000 spectral scans, and the signal-to-noise ratio ranges from 700:1 to 2000:1. Residuals are presented relative to the line profile amplitude at 42 Torr. Typical measurement time for one scan is 750 ms. The offset frequency of 203821.934011250 GHz is subtracted from the abscissa. **b**, Transitions in $H_2{}^{16}O$ and $HD^{16}O$ molecules that were included in the analysis of the HD P(3) 2-0 line. The rectangle indicates the spectral range of the HD line measurement. **c**, Line intensity measurement results of the HD spectrum from (**a**) and their comparison with the *ab initio* results[40,41]. The reference line intensity S^*corresponds to SDBBP$_{ab}$ analysis with a relative combined uncertainty of 1.23‰. Combined uncertainty includes both type A (fit uncertainty) and type B uncertainties. Results of analysis using qSDHCP, qSDHCP$_{ab}$ and SDBBP are also shown. Permille agreement with the *ab initio* intensity and shape of the HD line is presented.

significant contribution to the uncertainty budget of line intensity also comes from choosing the correct line-shape model. Accurate dispersive CRDS spectra can help in testing new theoretical models of intermolecular interactions and *ab initio* calculations of line intensities and line-shape parameters. As we have shown, the qSDHCP profile is no longer sufficient to accurately describe the shape of molecular hydrogen lines, and the more physical SDBBP should be used instead. The intensity of the HD line obtained using this model, combining *ab initio* line-shape parameters, agrees excellently with *ab initio*-calculated line intensity. Moreover, the results from Fig. 2c clearly show that agreement between the current most accurate experimental results for CO line intensity is better than their agreement with the most accurate *ab initio* result. Therefore, line intensities determined by our method can serve as a sub-‰ reference used in such important aplications as global GHG measurements, studies of the atmosphere of exoplanets or monitoring trace humidity in semiconductor production. Finally, the presented dispersive spectroscopy stimulates an area of research devoted to very accurate *ab initio* calculations of spectral line shapes and their intensities, which have implications for both fundamental science and many applications.

References

1. Fung, I. Y., Doney, S. C., Lindsay, K., John, J. Evolution of carbon sinks in a changing climate. *PNAS* **102**, 11201-11206 (2005).
2. Thompson, D. R. et al. Atmospheric validation of high accuracy CO_2 absorption coefficients for the OCO-2 mission. *J. Quant. Spectrosc. Radiat. Transfer* **113**, 2265-2276 (2012).
3. Coplen, T. B. et al. New guidelines for $\delta^{13}C$ measurements. *Anal. Chem.*. **78**, 2439-2441 (2006).
4. Fleisher, A. J. et al. Absolute $^{13}C/^{12}C$ isotope amount ratio for Vienna PeeDee Belemnite from infrared absorption spectroscopy. *Nat. Phys.* **17**, 889-893 (2021).
5. Fleisher, A. J. et al. Twenty-five-fold reduction in measurement uncertainty for a molecular line intensity. *Phys. Rev. Lett.* **123**, 043001 (2019).
6. Amato, L. S. et al. Linestrength ratio spectroscopy as a new primary thermometer for redefined Kelvin dissemination. *New J. Phys.* **21**, 113008 (2019).
7. Stock, M., Davis, R., de Mirandés, E. & Milton, M. J. T. The revision of the SI – the result of three decades of progress in metrology. *Metrologia* **56**, 022001 (2019).
8. Jousten, K. et al. Perspectives for a new realization of the pascal by optical methods. *Metrologia* **54**, S146-S161 (2017).
9. Egan, P. F. et al. Performance of a dual Fabry–Perot cavity refractometer. *Opt. Lett.* **17**, 3945 (2015).
10. Silander, I. et al. Invar-based refractometer for pressure assessments. *Opt. Lett.* **45**, 2652 (2020).
11. Słowiński, M. et al. H_2-He collisions: Ab initio theory meets cavity-enhanced spectra. *Phys. Rev. A* **101**, 052705-7 (2020).
12. Bielska, K. et al. Subpromille measurements and calculations of CO (3–0) overtone line intensities. *Phys. Rev. Lett.* **129**, 043002 (2022).
13. Polyansky, O. L. et al. High-accuracy CO_2 line intensities determined from theory and experiment. *Phys. Rev. Lett.* **114**, 243001 (2015).
14. O'Keefe, A. & Deacon, D. A. G. Cavity ringdown optical spectrometer for absorption measurements using pulsed laser sources. *Rev. Sci. Instrum.* **59**, 2544 (1988).
15. Long, D. A. et al. Frequency-stabilized cavity ring-down spectroscopy. *Chem. Phys. Lett.* **536**, 1-8 (2012).
16. Lin, H., Reed, Z. D., Sironneau, V. T. & Hodges, J. T. Cavity ring-down spectrometer for high-fidelity molecular absorption measurements. *J. Quant. Spectrosc. Radiat. Transfer* **161**, 11 (2015).
17. Maddaloni, P. et al. Absolute measurement of the S(0) and S(1) lines in the electric quadrupole fundamental band of D_2 around 3 μm. *J. Chem. Phys.* **133**, 154317 (2010).
18. Wójtewicz S. et al. Line-shape study of self-broadened O_2 transitions measured by Pound-Drever-Hall-locked frequency-stabilized cavity ring-down spectroscopy. *Phys. Rev. A* **84**, 032511 (2011).
19. Cygan, A. et al. One-dimensional frequency-based spectroscopy. *Opt. Express* **23**, 14472 (2015).
20. Cygan, A. et al. High-accuracy and wide dynamic range frequency-based dispersion spectroscopy in an optical cavity. *Opt. Express* **27**, 21810 (2019).
21. Cygan, A. et al. Cavity buildup dispersion spectroscopy. *Comm. Phys.* **4**, 1-9 (2021).
22. Levenson, M. D. et al. Optical heterodyne detection in cavity ring-down spectroscopy. *Chem. Phys. Lett.* **290**, 335-340 (1998).

Anodization-free fabrication process for high-quality cross-type Josephson tunnel junctions based on a Nb/Al-AlO$_x$/Nb trilayer

F Bauer[1,2], C Enss[1,3] and S Kempf[2,3,1]

[1] Kirchhoff-Institute for Physics, Heidelberg University, Im Neuenheimer Feld 227, D-69120 Heidelberg, Germany

[2] Institute of Micro- and Nanoelectronic Systems, Karlsruhe Institute of Technology, Hertzstrasse 16, Building 06.41, D-76187 Karlsruhe, Germany

[3] Institute for Data Processing and Electronics, Karlsruhe Institute of Technology, Hermann-von-Helmholtz-Platz 1, Building 242, D-76344 Eggenstein-Leopoldshafen, Germany

E-mail: fabienne.bauer@kit.edu

March 2024

Abstract. Josephson tunnel junctions form the basis for various superconducting electronic devices. For this reason, enormous efforts are routinely taken to establish and later on maintain a scalable and reproducible wafer-scale manufacturing process for high-quality Josephson junctions. Here, we present an anodization-free fabrication process for Nb/Al-AlO$_x$/Nb cross-type Josephson junctions that requires only a small number of process steps and that is intrinsically compatible with wafer-scale fabrication. We show that the fabricated junctions are of very high-quality and, compared to other junction types, exhibit not only a significantly reduced capacitance but also an almost rectangular critical current density profile. Our process hence enables the usage of low capacitance Josephson junctions for superconducting electronic devices such as ultra-low noise dc-SQUIDs, microwave SQUID multiplexers based on non-hysteretic rf-SQUIDs and RFSQ circuits.

Keywords: Josephson tunnel junctions, microfabrication process, Nb/Al-AlO$_x$/Nb trilayer, subgap leakage, thermal activation theory, unshunted dc-SQUIDs, capacitance measurements.

Aerosol Jet Printing of High-Temperature Multimodal Sensors for Strain and Temperature Sensing

*Md. Omarsany Bappy, Qiang Jiang, Stephanie Atampugre, and Yanliang Zhang**

Department of Aerospace and Mechanical Engineering, University of Notre Dame, Notre Dame, Indiana 46556, USA

KEYWORDS: multimodal sensors, thermocouples, nanoparticles, aerosol jet printing, printed sensors, high-temperature applications, health monitoring

ABSTRACT: Integrating multiple sensing capabilities into a single multimodal sensor greatly enhances its applications for in-situ sensing and structural health monitoring. However, the fabrication of multimodal sensors is complicated and limited by the available materials and existing manufacturing methods that often involve complex and expensive fabrication processes. In this study, a high-temperature multimodal sensor is demonstrated by aerosol jet printing of gold and ITO nanoparticle inks. The printed multimodal sensor for concurrent strain and temperature sensing possesses a high gauge factor of 2.54 and thermopower of 55.64 μV/°C combined with excellent high-temperature thermal stability up to 540 °C. Compared to traditional single-modality sensors, the printed multimodal sensor significantly increases sensing capacity and improves spatial resolution using microscale printed patterns. The study also demonstrates that the strain sensor with integrated thermocouple enables in-situ compensation of the temperature effect on strain sensing, significantly improving strain measurement accuracy at high temperatures. By

First-principle event reconstruction by time-charge readouts for the Taishan Antineutrino Observatory

Xuewei Liu[a,b,c], Wei Dou[a,b,c], Benda Xu[a,b,c,d], Hanwen Wang[e], Guofu Cao[e]

[a] *Department of Engineering Physics, Tsinghua University, Beijing, China*
[b] *Center for High Energy Physics, Tsinghua University, Beijing, China*
[c] *Key Laboratory of Particle & Radiation Imaging (Tsinghua University), Ministry of Education, China*
[d] *Kavli Institute for the Physics and Mathematics of the Universe, UTIAS, the University of Tokyo, Tokyo, Japan*
[e] *Institute of High Energy Physics, Chinese Academy of Sciences, Beijing, China*

Abstract

The Taishan Antineutrino Observatory (TAO) is a liquid-scintillator satellite experiment of the Jiangmen Underground Neutrino Observatory (JUNO) to measure the reference reactor neutrino spectrum with sub-percent energy resolution. We use inhomogeous Poisson process and Tweedie generalized linear model (GLM) to calibrate the detector response and the charge distribution of a SiPM. We develop a pure probabilistic method using time and charge of SiPMs from first principles to reconstruct point-like events in the TAO central detector. Thanks to our precise model and the high photo-coverage and quantum efficiency of the SiPM tiles at TAO, we achieve a vertex position resolution better than 16 mm and an energy resolution of about 2 % at 1 MeV, marking the world's best performance of liquid scintillator detectors. Our methodology is applicable to other experiments that utilize PMTs for time and charge readouts.

1. Introduction

The Taishan Antineutrino Observatory (TAO) is a satellite experiment of the Jiangmen Underground Neutrino Observatory (JUNO) [1]. Using 2.8 tons Gadolinium-doped Liquid Scintillator (GdLS) and 4024 Silicon Photomultiplier (SiPM) tiles, TAO will measure the neutrino energy spectrum from a reactor core of the Taishan Nuclear Power Plant 44 m away. It will provide a model-independent reference spectrum with an energy resolution about 2 % at 1 MeV. The spectra predicted by reactor flux models disagree with the measured ones by Daya Bay and other rector antineutrino experiments, due to the incomplete information of decay and fission yields in nuclear database [2]. Thus, the precisely measured spectra of reactor antineutrino would provide more reliable inputs to JUNO for determining the neutrino mass ordering. Such reference spectra can also benchmark the nuclear database. In order to achieve these goals, <1 % uncertainty in the physics non-linearity and <0.5 % residual non-uniformity are required in TAO, supported by the study of calibration strategy [1].

Many reconstruction methods have been developed for large liquid scintillation and water Cherenkov detectors. Usually, the arrival time of the first photo-electron (PE) and the total integrated charge, collectively referred to as time-charge, in a chunk of PMT/SiPM readout waveforms, are used as substitutes for raw data in the event reconstruction. The time distribution of the first PE is long known to be affected by PE pile-up [3, 4]. KamLAND [5] uses a time-only vertex fitter with heuristic corrections. The Borexino [6] and Super-Kamiokande [7] experiments construct several empirical first-PE time PDFs from calibration and Monte Carlo conditioned by different charges and interpolate during reconstruction. In Ziyuan Li et al. [8]'s study of event reconstruction for JUNO, a rigorous time dependence on the PE counts is used, but they are inaccurately estimated by charge rounding. Guihong Huang et al. [9] improve upon it by relying on both the expectation of PE count and PE count itself. But the time-charge-combined likelihood is a simplified direct product of the two components. Such approximations introduce inherent bias needing to be *ad-hocly* corrected *a posteriori*. Zhen Qian et al. [10] discuss the application of several machine learning models in the reconstruction. The performance of these methods depends on the selection of aggregated features and optimal hyperparameters. Lacking of interpretability, deep learning is still seen as a black box for many applicaitons [11].

[1]Long-Distance Signal Propagation in AC-LGAD

C. Bishop, A. Das, J. Ding, M. Gignac, F. Martinez-McKinney, S. M. Mazza, A. Molnar, N. Nagel, M. Nizam, J. Ott, H. F.-W. Sadrozinski, B. Schumm, A. Seiden, T. Shin, A. Summerell, M. Wilder, Y. Zhao

SCIPP, Univ. of California Santa Cruz, CA 95064, USA

Abstract– We investigate the signal propagation in AC-LGAD (aka RSD), which are LGAD with a common N^+ layer and segmented AC-coupled readout contacts, by measuring response to IR laser TCT on a large selection of AC-LGAD with strip readout. The interest for this topic derives from the realization that while large charge sharing between neighboring strips is essential for good position resolution, large sharing beyond the next neighbor generates background signals which in general are detrimental to the sensor goal of low occupancy. Using AC-LGAD with strip readout produced by Hamamatsu Photonics (HPK), we evaluate the effects of a variety of sensor properties, including geometrical parameters (strip length, width), process parameters like the N^+ layer resistivity, the coupling capacitance, and the thickness of the bulk on the signal sharing and the position resolution.

PACS: 29.40.Gx, 29.40.Wk, 78.47jc

Keywords: fast silicon sensors; charge multiplication; AC-LGAD strips; charge sharing.

1. Introduction

Low-gain Avalanche Detectors (LGAD) have been recently introduced as fast semiconductor timing sensors [1,2]. In their experimental applications their segmentation is limited to pads with 1 mm pitch by consideration of power and fill-factor. To avoid this restriction which limits the spatial resolution, the AC-LGAD technology (aka Resistive Silicon Detector RSD) [3-5] is under investigation, based on a complete integration of four of the sensor layers in common sheets of the P-type bulk, the P^+ gain layer, the N^+ layer and a dielectric sheet, separating the first three from the segmented metal readout contacts (Fig. 1). A signal originating in the bulk and amplified in the gain layer is then shared between several electronics channels, allowing reconstruction of signal location with a resolution which is a small fraction of the readout pitch. Yet due to the common N^+ layer, the observed signal in AC-LGADs is the sum of the directly induced signal from the moving collected charge on neighboring contacts (shown in red in Fig. 1) and the pick-up of the signal conducted on the N^+ layer common to all contacts ("leakage" shown in yellow).
The relative strength between induced and conducted signal depends on a variety of sensor parameters which we compare in the following study using scanning laser Transient Current Technique (TCT) on strip AC-LGAD produced by HPK : the geometry of the metal readout contacts was varied, as were production details of two common layers (N^+ layer resistivity and dielectric specs) and the bulk thickness. The doping

Presentation at the 13th "Hiroshima" Symposium HSTD13 in Vancouver, CA, Dec. 2013

A clear case for dust obscuration of the lunar retroreflectors

Sanchit Sabhlok[a,*], James B. R. Battat[c], Nicholas R. Colmenares[d], Daniel P. Gonzales[a,e] and Thomas W. Murphy, Jr.[b]

[a]Department of Physics, University of California San Diego, 9500 Gilman Drive, La Jolla, 92093-0424, CA, USA
[b]Department of Astronomy and Astrophysics, University of California San Diego, 9500 Gilman Drive, La Jolla, 92093-0424, CA, USA
[c]Department of Physics and Astronomy, Wellesley College, 106 Central Street, Wellesley, 02481, MA, USA
[d]Geodesy and Geophysics Lab, NASA Goddard Space Flight Center, 8800 Greenbelt Rd., Greenbelt, 20771, MD, USA
[e]Department of Physics, University of Maryland Baltimore County, 1000 Hilltop Circle, Baltimore, 21250, MD, USA

ARTICLE INFO

Keywords:
Eclipses
Moon, surface
Regoliths

ABSTRACT

The passive retroreflector arrays placed on the moon by Apollo 11, 14 and 15 astronauts continue to produce valuable Earth-Moon range measurements that enable high-precision tests of gravitational physics, as well as studies of geo- and selenophysics. The optical throughput of these retroreflectors has declined since their deployment, with an additional signal loss at full moon when the reflectors experience direct solar illumination. We show that the loss in return rate can be attributed to the accumulation of a thin layer of lunar dust on the surfaces of the corner cube retroreflectors. First, a careful analysis of the optical link budget for the Apache Point Observatory Lunar Laser-ranging Operation (APOLLO) experiment reveals that the lunar return rate is 15–20 times smaller than predicted, a deficit that can be explained by a reflector dust covering fraction of ∼50%. Second, range measurements taken during a lunar eclipse indicate that the solar illumination of the retroreflectors degrades their throughput by an additional factor of ∼15. Finally, a numerical simulation of heat transfer in dust-coated reflectors is able to model the resulting thermal lensing effect, in which thermal gradients in the retroreflectors degrade their far-field diffraction pattern. A comparison of this simulation to eclipse measurements finds a dust coverage fraction of ∼50%. Taken together, the link analysis, eclipse observations and thermal modeling support the claim that the retroreflectors are obscured by lunar dust, with both link budget and simulation independently finding the dust fraction to be ∼50%.

1. Introduction

The corner cube reflectors (CCRs) placed on the moon by Apollo 11, 14 and 15 astronauts continue to produce scientific output more than 50 years after their deployment. The reflectors were designed to sit passively in the periodic temperature swings of the lunar environment in order to facilitate Lunar Laser Ranging (LLR) measurements. It would be fair to say that these reflectors have greatly outperformed expectations, continuing to operate for more than 50 years after placement. Measurements of the Earth–Moon distance provide precision tests of fundamental physics (e.g. general relativity, Lorentz Invariance, time evolution of fundamental constants), as well as geophysical information and constraints on the composition and dynamics of the lunar interior (Murphy 2013).

The Apache Point Observatory Lunar Laser-ranging Operation (APOLLO) began its science campaign in 2006 (Murphy et al. 2008) with the goal of providing millimeter-accuracy range data to improve constraints on gravitational physics.

When APOLLO started ranging, it became clear that the measured return signal was lower than expected by about a factor of 10 from careful link budget calculations (Murphy et al. 2007). Surprisingly, the signal fell by an additional order of magnitude when the lunar phase was within ∼ 20° of full moon (Murphy et al. 2010). Murphy et al. (2010) discussed various scenarios that could lead to the degradation of performance over four decades in the lunar environment, the favored scenario being deposition of dust on the retroreflector surfaces. In a subsequent work, Goodrow and Murphy showed that thermal gradients of a few degrees in a CCR would lead to dramatic suppression of the central intensity of the far-field diffraction pattern (FFDP) Goodrow and Murphy (2012). While this does imply that the return signal from the reflectors would be lowered as a result of a thermal gradient, the paper did not perform any thermal modelling of the CCR under solar illumination.

ssabhlok@ucsd.edu (S. Sabhlok)
ORCID(s): 0000-0002-8780-8226 (S. Sabhlok); 0000-0003-1236-1228 (J.B.R. Battat); 0009-0008-6736-557X (N.R. Colmenares); 0009-0008-0789-2052 (D.P. Gonzales); 0000-0003-1591-6647 (T.W.M. Jr.)

Optical-coherence-tomography-based deep-learning scatterer-density estimator using physically accurate noise model

THITIYA SEESAN,[1] PRADIPTA MUKHERJEE,[1] IBRAHIM ABD EL-SADEK,[1,2] YIHENG LIM,[1] LIDA ZHU,[1] SHUICHI MAKITA,[1] AND YOSHIAKI YASUNO[1,*]

[1]*Computational Optics Group, University of Tsukuba, Tsukuba, Ibaraki 305-8573, Japan*
[2]*Department of Physics, Faculty of Science, Damietta University, New Damietta City 34517, Damietta, Egypt*
[*]*yoshiaki.yasuno@cog-labs.org*
https://cog-news.blogspot.com/

Abstract: We demonstrate a deep-learning-based scatterer density estimator (SDE) that processes local speckle patterns of optical coherence tomography (OCT) images and estimates the scatterer density behind each speckle pattern. The SDE is trained using large quantities of numerically simulated OCT images and their associated scatterer densities. The numerical simulation uses a noise model that incorporates the spatial properties of three types of noise, i.e., shot noise, relative-intensity noise, and non-optical noise. The SDE's performance was evaluated numerically and experimentally using two types of scattering phantom and *in vitro* tumor spheroids. The results confirmed that the SDE estimates scatterer densities accurately. The estimation accuracy improved significantly when compared with our previous deep-learning-based SDE, which was trained using numerical speckle patterns generated from a noise model that did not account for the spatial properties of noise.

1. Introduction

Optical coherence tomography (OCT) is a non-invasive imaging modality that is used to provide high-resolution structural information about biological tissues [1–3]. The anatomical images provided by OCT are used widely in clinical diagnosis [4].

In addition to anatomical investigations, OCT-based assessments of the optical properties of tissue have also been studied and have provided useful biomarkers. One commonly investigated optical property of biological tissues is the attenuation coefficient (AC) [5, 6], and the AC is considered to be related to the tissue density. AC measurements are useful in a wide variety of applications, including investigation of tumor spheroid necrosis [7, 8] and distinguishing between normal and cancerous tissues [9–11]. However, AC measurements are strongly influenced by the measurement configuration and conditions, which including the system confocality, the depth position of the focus, and the presence of aberrations [12–14], and these factors can limit the accuracy and reliability of the AC measurements. Although several methods have been proposed to compensate for these effects, they generally require hard-wired assumptions to be made [12] or multiple measurements to be performed [15].

Rather than use the AC to assess biological tissue density, we have proposed a deep-learning based method that estimates the scatterer density of the tissue directly [16–18]. In this work, we denote this method as the scatterer density estimator (SDE). The SDE analyzes the local spatial patterns of an OCT intensity image, i.e., the speckle pattern, using a convolutional neural network (CNN) and then estimates the scatterer density. The CNN was trained using fully numerically simulated OCT speckle patterns that were generated by a simple scalar-optics-based OCT simulator. This approach provides significant amounts of training data, and the data sets reflect the variety of the parameters involved in OCT imaging, including the resolution, the

Improved Modelling of Detector Response Effects in Phonon-based Crystal Detectors used for Dark Matter Searches

M. J. Wilson,[1,*] A. Zaytsev,[1,†] B. von Krosigk,[2] I. Alkhatib,[3] M. Buchanan,[3] R. Chen,[4] M.D. Diamond,[3] E. Figueroa-Feliciano,[4] S.A.S. Harms,[3] Z. Hong,[3] K.T. Kennard,[4] N.A. Kurinsky,[5] R. Mahapatra,[6] N. Mirabolfathi,[6] V. Novati,[4,‡] M. Platt,[6] R. Ren,[3] A. Sattari,[3] B. Schmidt,[4,§] Y. Wang,[3] S. Zatschler,[3,‡] E. Zhang,[3] and A. Zuniga[3]

[1] *Institut für Astroteilchenphysik, Karlsruher Institut für Technologie, 76133 Karlsruhe, Germany*
[2] *Kirchhoff-Institut für Physik, Universität Heidelberg, 69117 Heidelberg, Germany*
[3] *Department of Physics, University of Toronto, Toronto, ON M5S 1A7, Canada*
[4] *Department of Physics & Astronomy, Northwestern University, Evanston, IL 60208-3112, USA*
[5] *SLAC National Accelerator Laboratory/Kavli Institute for Particle Astrophysics and Cosmology, Menlo Park, CA 94025, USA*
[6] *Department of Physics and Astronomy, and the Mitchell Institute for Fundamental Physics and Astronomy, Texas A&M University, College Station, TX 77843, USA*

(Dated: March 5, 2024)

Various dark matter search experiments employ phonon-based crystal detectors operated at cryogenic temperatures. Some of these detectors, including certain silicon detectors used by the SuperCDMS collaboration, are able to achieve single-charge sensitivity when a voltage bias is applied across the detector. The total amount of phonon energy measured by such a detector is proportional to the number of electron-hole pairs created by the interaction. However, crystal impurities and surface effects can cause propagating charges to either become trapped inside the crystal or create additional unpaired charges, producing non-quantized measured energy as a result. A new analytical model for describing these detector response effects in phonon-based crystal detectors is presented. This model improves upon previous versions by demonstrating how the detector response, and thus the measured energy spectrum, is expected to differ depending on the source of events. We use this model to extract detector response parameters for SuperCDMS HVeV detectors, and illustrate how this robust modelling can help statistically discriminate between sources of events in order to improve the sensitivity of dark matter search experiments.

I. INTRODUCTION

Cryogenic solid-state detectors are used in a number of dark matter (DM) search experiments [1–6]. In these experiments, incoming DM particles are expected to scatter off of the detector nuclei or electrons, creating phonon signals which are measured by high resolution phonon sensors. Resolution on the order of 1 eV is achieved, which allows for reduced energy thresholds and enables the detection of nuclear recoils with energies as low as ∼10 eV [1–3]. Low-mass DM candidates that produce small interaction energies can be probed via electron recoils by measuring the ionization signal — the number of produced e^-h^+ pairs in the detector [7, 8]. In phonon-based crystal detectors, when a voltage bias is applied across the crystal, the ionization signal is converted into an amplified phonon signal via the Neganov-Trofimov-Luke (NTL) effect [9, 10]. A charge carrier with a charge e accelerated by the electric field scatters off of the crystal lattice and produces NTL phonons with the total energy equal to the work done by the electric field to move the charge through the electric potential difference $\Delta\varphi$:

$$E_{\mathrm{NTL}} = e\,\Delta\varphi. \tag{1}$$

Normally, when an e^-h^+ pair is created in the crystal, each charge drifts in the electric field all the way to the corresponding electrode on the crystal surface. Together they traverse the entire voltage bias of the detector, so the total energy of the produced NTL phonons is given by:

$$E_{\mathrm{NTL}} = n_{\mathrm{eh}} e V_{\mathrm{bias}}, \tag{2}$$

where n_{eh} is the number of e^-h^+ pairs and V_{bias} is the voltage bias. The total phonon energy produced in an event is then given by:

$$E_{\mathrm{ph}} = E_{\mathrm{dep}} + n_{\mathrm{eh}} e V_{\mathrm{bias}}, \tag{3}$$

where E_{dep} is the energy deposited in the detector by the incoming particle. For a detector with a good phonon energy resolution σ_{res} and a large voltage bias, where $\sigma_{\mathrm{res}} \ll eV_{\mathrm{bias}}$, the spectrum of the phonon energy in Eq. 3 is expected to have quantized peaks corresponding to the integer number of created e^-h^+ pairs. This e^-h^+-pair quantization is observed in SuperCDMS high-voltage (HV) and HV eV-scale (HVeV) detectors when operated with a voltage bias on the order of 100 V [7, 8, 11].

Due to the presence of impurities in the crystal, non-quantized amount of NTL energy can be produced in an event. We distinguish two categories of effects causing non-quantized NTL energy: charge trapping (CT) and impact ionization (II). In a CT process, a charge carrier gets trapped in an impurity state in the bulk of the crystal. In an II process, a propagating charge ejects (or

* matthew.wilson@kit.edu
† alexander.zaytsev@kit.edu
‡ Presently at LPSC, CNRS, Université Grenoble Alpes, Grenoble, France
§ Presently at IRFU, CEA, Université Paris-Saclay, France

Electron Spectroscopy using Transition-Edge Sensors

K. M. Patel,[1,2] S. Withington,[3] A. G .Shard,[2] D. J. Goldie,[1] and C. N. Thomas[1]
[1)] *Cavendish Laboratory, University of Cambridge, JJ Thomson Avenue, Cambridge CB3 0HE, United Kingdom*
[2)] *National Physical Laboratory, Hampton Road, Teddington TW11 0LW, United Kingdom*
[3)] *Department of Physics, University of Oxford, Oxford OX1 3PU, United Kingdom*

(Dated: 5 March 2024)

Transition-edge sensors (TESs) have the potential to perform electron spectroscopic measurements with far greater measurement rates and efficiencies than can be achieved using existing electron spectrometers. Existing spectrometers filter electrons by energy before detecting a narrow energy band at a time, discarding the vast majority of electrons available for measurement. In contrast, transition-edge sensors (TES) have intrinsic energy sensitivity and so do not require prior filtering to perform energy-resolved measurements. Despite this fundamental advantage, TES electron spectroscopy has not, to our knowledge, previously been reported in the literature. We present the results of a set of proof-of-principle experiments demonstrating TES electron spectroscopy experiments using Mo/Au TESs repurposed for electron calorimetry. Using these detectors, we successfully measured the electron spectrum generated by an electron beam striking a graphite target with energies between 750 and 2000 eV, at a noise-limited energy resolution of 4 eV. Based on the findings of these experiments, we suggest improvements that could be made to TES design to enhance their electron detection capabilities through the use of of a dedicated electron absorber in the device with integrated electron optics.

I. INTRODUCTION

Transition-edge sensors (TESs) are thin-film superconducting devices capable of high-sensitivity, energy-resolved photon measurement. Over the last thirty years, TESs have found applications across an increasing range of fields from astronomic observations to dark matter searches[1–6]. However, one area of TES research that has received little attention is massive particle spectroscopy, encompassing molecular, ion-beam and electron measurement techniques. The lack of research into TES electron spectroscopy is of particular note due to the widespread usage of electron spectroscopic techniques and the potential benefits offered by TESs over conventional electron spectrometers.

All modern commercial electron spectrometers follow the same fundamental operating principle where electrons are collected, dispersed by energy and then counted using energy-insensitive detectors. For example, the concentric hemispherical analyser (CHA), the analyser of choice for X-ray photoelectron spectroscopy (XPS) measurements, uses the electric field between two concentric hemispheres of differing electric potentials to disperse electrons in space depending on their energy. This arrangement sets up an energy filter where only electrons within a narrow energy band, defined by the hemisphere potentials, can pass through the hemispheres to the particle-counting microchannel plate.

The inefficiency in this form of measurement lies in the fact that only a narrow electron energy band, approximately 1 to 10 eV in width, can be measured at a time. To perform a wide spectrum measurement, this narrow band must be swept across the entire spectral range and so, at every individual moment in time, the vast majority of electrons emitted from the sample and collected by the instrument cannot be measured. If an energy range of 1 keV is to be measured, a CHA measuring a window of 1 eV would have at best a measurement efficiency of 0.1 % across the measurement. The effect of this inefficiency can be mitigated by increasing the number of electrons collected, either by emitting more electrons from the sample or widening the solid angle of collection; however, these measures cannot address the underlying inefficiency within the operating principle of the spectrometer itself.

An alternate approach is time-of-flight electron spectrometry[7]. In this case, a pulsed X-ray source is required and this is only achievable with specialized and expensive equipment such as an X-ray Free Electron Laser (XFEL). The operation requires fast detection electronics and the electron time-of-flight can be converted into kinetic energy, which scales as the inverse square of the flight time. In principle, all emitted electrons entering the analyzer can be detected, but with variable energy resolution which depends upon the pulse width of the X-ray source, the detector electronics and the time of flight. Only low-energy electrons are detected with good energy resolution and thus the electrons are typically retarded using an electric field prior to entering the analyzer. For practical purposes, the efficiency, resulting from the duty cycle of X-rays and the necessity to collect multiple kinetic energy regions, is low.

The ideal solution is to use a detector that is intrinsically able to resolve the energy of an incident electron, removing the need for filtering in space or time. Such a detector would be capable of continuous measurement and the instantaneous fraction of electrons emitted from the sample that can be characterized will scale with the number of detectors used. TESs are near-ideal candidate, as they have high energy sensitivities and the technology exists to readout out arrays of several thousand devices concurrently[8–10].

TESs perform high-resolution particle calorimetry by

ee∈MC: Comments on Asymmetries in QED

Ian M. Nugent*
Victoria, B.C., Canada

Abstract

In the Quantum Electrodynamics process $e^+e^-\to l^+l^-(n\gamma)$, there are two well known angular asymmetries in the $cos(\theta)$ and the $cos(\theta^*)$ distributions. In this paper, the QED angular asymmetry related to the $cos(\theta^*)$ distribution is investigated in terms of the Dirac propagator and the associated boundary conditions from which the Dirac propagator is constructed and the potential implications are examined.

Keywords: Electron-Positron Collider, Tau Lepton, Monte-Carlo Simulation

1 Introduction

In Quantum Electrodynamics (QED) processes, the higher order emission of hard photons directly influences the angular dependence in the differential cross-section. Consequently, for the $e^+e^-\to\mu^+\mu^-(\gamma)$ and $e^+e^-\to\tau^+\tau^-(\gamma)$ processes, this is related to the angular asymmetry between the outgoing charged leptons $cos(\theta)$ [1, 2, 3, 4, 5, 6, 7] and $cos(\theta^*)$ [8], asymmetry in the angle between the outgoing lepton and the radiated hard photon in the center-of-mass frame of the outgoing lepton pair. Higher order contributions, in particular, Feynman Diagrams with k=2, ... internal photon exchanges further modify the $cos(\theta)$ asymmetry [9][1], where the virtual and soft-photon contributions are most significant. This is in contrast to the $cos(\theta^*)$ angular distributions, where the asymmetry originates from the inclusion of Feynman Diagrams that contain n=1 or more real hard photon emissions. In $ee\in MC$ [10], each of the hard matrix elements, $\mathcal{M}_n^k$ for n real hard photon emissions and k internal photon exchanges, are explicitly calculated without approximations from the Gamma-Matrices and Dirac spinors using an object-oriented structure. This allows for the investigation of the angular asymmetry $cos(\theta^*)$ in terms of the treatment of the Dirac propagator and the associated boundary conditions.

2 Overview of ee∈MC Formalism

The ee∈MC [10] Monte-Carlo generator, is a stand-alone software program which contains the random-number generation [11, 12, 13, 14, 15], the phase-space generation [10, 16] based on the [17] algorithm modified to include embedded importance sampling [18, 19] and the theoretical models for the QED processes $e^-e^+\to\mu^+\mu^-(n\gamma)$, $e^-e^+\to\tau^+\tau^-(n\gamma)$, $e^-e^+\to hadrons(n\gamma)$ and τ lepton decays. The cross-section for the QED processes $e^-e^+\to\mu^+\mu^-(n\gamma)$, $e^-e^+\to\tau^+\tau^-(n\gamma)$ and $e^-e^+\to hadrons(n\gamma)$ is constructed within the Yennie-Frautschi-Suura (YFS) Exponentiation Formalism [20] for the infra-red subtraction

$$d\sigma=\frac{\sum_{n=0}^{\infty}\Pi_{i=0}^{n}\Pi_{j=0}^{j<i}F\left(Y_{i,j}^{\mathcal{O}(\alpha)}(P_i^{\mu},P_j^{\mu})\right)|\sum_{k=1}^{\infty}\bar{\mathcal{M}}_n^k|^2dPS_n}{4(|\vec{P}_{e^-}\ |E_{e^+}+E_{e^-}|\vec{P}_{e^+}|)} \tag{1}$$

where $F(x)$ is some functional form representing the resummation of all permutations for soft or virtual photon exchanges. For the Initial and Final YFS multiplicative subtraction, the function form $F(x)$ is the standard exponential YSF Form-Factor for the Yennie-Frautschi-Suura calculation [20]; the KK2F approximation [21]; and the Sudakov Form-Factor [3]. For the Full LO calculation from [22] applying corrections from [3, 10, 23], the $F(x)$ is the product of the exponential Form-Factor determined from [22] with the Coulomb potential factored out into a separate multiplicative resummation series, the Sommerfeld-Sakharov resummation factor [23]. The hard matrix elements, $\bar{\mathcal{M}}_n^k$, is determined with the spin-average-sum for an arbitrary Initial-State spin configuration [24] and is explicitly determined from the Feynman calculus corresponding to each Feynman Diagrams using an object-orientated representation of the Gamma-Matrices and Dirac Spinors [10]. Ward's Identity [6] is applied to incorporate the renormalization through the running of electromagnetic coupling constant [10, 25, 26]. Details on the simulation of the τ decays can be found in [10, 27].

3 Dirac Propagator Formalism

It is well known that the Dirac propagator can be described in terms of the retarded Green's function for a free particle with retarded boundary conditions [3],

$$G=\imath<0|\{\psi_a(x')\bar{\psi}_b(x)\}|0>\theta(x'_{(0)}-x_{(0)}). \tag{2}$$

From which it follows that:

$$\left(\imath\gamma^{\mu}\tfrac{\partial}{\partial x'_{\mu}}-m\right)G(x'-x)=\delta^4(x'-x). \tag{3}$$

*Corresponding Author
Email: inugent.physics@outlook.com

[1] These are the most significant terms in the infinite perturbative series.

Quantum-enhanced sensing of axion dark matter with a transmon-based single microwave photon counter

C. Braggio[1,2,*], L. Balembois[3], R. Di Vora[4],
Z. Wang[3], G. Carugno[2], A. Ortolan[4], G. Ruoso[4], U. Gambardella[5], D. D'Agostino[5],
P. Bertet[3], E. Flurin[3,*]

[1] Dipartimento di Fisica e Astronomia, Padova, Italy
[2] INFN, Sezione di Padova, Padova, Italy
[3] Quantronics group, Université Paris-Saclay, CEA, CNRS, SPEC, 91191 Gif-sur-Yvette Cedex, France
[4] Laboratori Nazionali di Legnaro, Legnaro, Padova, Italy
[5] INFN, Sezione di Napoli, Napoli, Italy

*To whom correspondence should be addressed;
e-mail: caterina.braggio@unipd.it, emmanuel.flurin@cea.fr.

We report an axion dark matter search with a haloscope equipped with a microwave photon counter. The haloscope is a tunable high quality factor 3-dimensional microwave cavity placed in a magnetic field. The photon counter, operated cyclically, maps an incoming microwave photon onto the state of a superconducting transmon qubit. The measurement protocol continuously monitors the power emitted by the haloscope cavity as well as the dark count background, and enables tuning of the cavity frequency to probe different axion masses. With this apparatus we enhance by a factor 20 the search speed that can be reached with quantum-limited linear amplifiers, and set a new standard for probing the existence of axions with resonant detectors.

PROCEEDINGS OF SCIENCE

Towards a SM prediction for CP violation in charm

Alexander Lenz,[a] **Maria Laura Piscopo**[a,*] **and Aleksey V. Rusov**[a]

[a] *Theoretische Teilchenphysik, Center for Particle Physics Siegen, Physik Department, Universität Siegen, Walter-Flex-Str. 3, 57068 Siegen, Germany*

E-mail: alexander.lenz@uni-siegen.de, maria.piscopo@uni-siegen.de, rusov@physik.uni-siegen.de

We provide an overview of the current experimental and theoretical status of charm CP violation and discuss recent progress in obtaining a Standard Model prediction for $\Delta a_{\rm CP}^{\rm dir}$ using the framework of light-cone sum rules. Furthermore, we present new results for the ratios of the direct CP asymmetries and of the branching fractions for the modes $D^0 \to \pi^+\pi^-$ and $D^0 \to K^+K^-$.

20th International Conference on B-Physics at Frontier Machines (Beauty2023)
3-7 July, 2023
Clermont-Ferrand, France

*Speaker

https://pos.sissa.it/

1. Introduction

The charm sector offers a unique system for testing the Standard Model of particle physics (SM), see Ref. [1] for a recent review. The peculiarities of charm are twofold. On the one hand, achieving precise theoretical predictions for charm observables is currently very challenging. This follows from the value of the charm quark mass which lies at the boundary between the heavy and the light quark regimes, such that the typical theoretical methods employed for the study of heavy hadrons might be less suitable or even inapplicable for the description of charmed systems. The behaviour of both the perturbative and power expansions becomes, in fact, a priori questionable as

$$\alpha_s(m_c) \sim 0.35\,, \qquad \frac{\Lambda_{\rm QCD}}{m_c} \sim 0.30\,. \tag{1}$$

On the other hand, charmed hadrons provide essential complementary information with respect to kaon- and b-physics, constituting, for instance, the only system to study meson-mixing in the up-quark sector. Additionally, the sensitivity to potential new physics (NP) contributions is high for charm observables, as pronounced cancellations often affect their SM predictions. The latter follow from the Glashow-Iliopoulos-Maiani (GIM) mechanism due to $m_b, m_s, m_d \ll m_W$, as well as from the size of the relevant elements of the Cabibbo-Kobayashi-Maskawa (CKM) matrix i.e. $\lambda_q \equiv V_{cq}^* V_{uq}$, namely

$$\lambda_d = -0.21874 + 2.51 \times 10^{-5} i\,, \qquad \lambda_s = 0.21890 + 0.13 \times 10^{-5} i\,, \tag{2}$$

$$\lambda_b = 6.3 \times 10^{-5} - 1.4 \times 10^{-4} i\,. \tag{3}$$

In particular, having λ_b the biggest relative imaginary part but being much smaller in magnitude compared to $\lambda_{d,s}$, the amount of CP violation in the charm sector is expected to be small in the SM. Testing this result against the experimental data, although theoretically difficult, is clearly a task of primary importance in order to strengthen the current understanding of the SM and search for NP.

2. Experimental status of CP violation in charm

The observation of CP violation in the charm sector was made in 2019 by the LHCb Collaboration [2], by measuring the difference of the time-integrated CP asymmetries in the $D^0 \to K^+K^-$ and $D^0 \to \pi^+\pi^-$ modes, that is $\Delta A_{\rm CP} \equiv A_{\rm CP}(K^+K^-) - A_{\rm CP}(\pi^+\pi^-)$. The corresponding difference of the direct CP asymmetries in the above channels turned out to be

$$\Delta a_{\rm CP}^{\rm dir}\big|_{\rm exp} = (-15.7 \pm 2.9) \times 10^{-4}\,. \tag{4}$$

Recently, also a measurement of the CP asymmetry in $D^0 \to K^+K^-$ was published by the LHCb Collaboration [3], which yields, when combined with the result in Eq. (4), the following values for the direct CP asymmetries in the two individual modes, namely

$$a_{\rm CP}^{\rm dir}(K^+K^-)\big|_{\rm exp} = (7.7 \pm 5.7) \times 10^{-4}\,, \qquad a_{\rm CP}^{\rm dir}(\pi^+\pi^-)\big|_{\rm exp} = (23.2 \pm 6.1) \times 10^{-4}\,. \tag{5}$$

While the result for $a_{\rm CP}^{\rm dir}(\pi^+\pi^-)$ provides the first evidence for CP violation in a specific D-meson decay, a clear theoretical interpretation of the measurements in Eqs. (4), (5) is currently still missing, particularly as the values of the individual CP asymmetries in Eq. (5) would imply a surprisingly large breaking of the U-spin symmetry [4].

The Z_b states as the mixture of the molecular and diquark-anti-diquark components within the effective field theory

Wei He[1,2],* De-Shun Zhang[1,2],† and Zhi-Feng Sun[1,2,3,4‡]
[1] *School of Physical Science and Technology, Lanzhou University, Lanzhou 730000, China*
[2] *Research Center for Hadron and CSR Physics, Lanzhou University and Institute of Modern Physics of CAS, Lanzhou 730000, China*
[3] *Lanzhou Center for Theoretical Physics, Key Laboratory of Theoretical Physics of Gansu Province, and Key Laboratory of Quantum Theory and Applications of the Ministry of Education, Lanzhou University, Lanzhou, 730000, China*
[4] *Frontiers Science Center for Rare Isotopes, Lanzhou University, Lanzhou, Gansu 730000, China*
(Dated: March 5, 2024)

In this study, we reconsider the states $Z_b(10610)$ and $Z_b(10650)$ by investigating the presence of diquark-anti-diquark components as well as the hadronic molecule components in the framework of effective field theory. The different masses of pseudoscalar mesons such as π^0, η_8, and η_0, as well as vector mesons like ρ^0 and ω violate the OZI rule that is well depicted under the $[U(3)_L \otimes U(3)_R]_{global} \otimes [U(3)_V]_{local}$ symmetry. To account for the contribution of intermediate bosons of heavy masses within the OBE model, we introduce an exponential form factor instead of the commonly used monopole form factor in the past. By solving the coupled-channel Schrödinger equation with the Gaussian expansion method, our numerical results indicate that the $Z_b(10610)$ and $Z_b(10650)$ states can be explained as hadronic molecules slightly mixing with diquark-anti-diquark states.

PACS numbers:

I. INTRODUCTION

In the past decades, a series of quarkonium-like states were discovered. In the $b\bar{b}$ sector, Belle Collaboration reported two charged bottomonium-like states which are known as $Z_b(10610)$ and $Z_b(10650)$ [1] in 2011. Both of them were observed in $\Upsilon(5S) \to \pi^{\pm} h_b(mP)$ $(m = 1, 2)$ and $\Upsilon(5S) \to \pi^{\pm}\Upsilon(nS)$ $(n = 1, 2, 3)$, respectively. Later, Belle confirmed their observations [2, 3]. The next year of the first discovery, the neutral state $Z_b^0(10610)$ was found in the $\Upsilon(5S) \to \Upsilon(2S, 3S)\pi^0\pi^0$ decay [4]. The masses and widths of these states listed in PDG (Particle Data Group) are shown below

$$\begin{aligned} M_{Z_b^{\pm}} &= 10607.2 \pm 2.0 \text{ MeV}, \quad \Gamma_{Z_b^{\pm}} = 18.4 \pm 2.4 \text{ MeV}, \\ M_{Z_b^0} &= 10609 \pm 4.0 \pm 4 \text{ MeV}, \\ M_{Z_b'^{\pm}} &= 10652.2 \pm 1.5 \text{ MeV}, \quad \Gamma_{Z_b'^{\pm}} = 11.5 \pm 2.2 \text{ MeV} \end{aligned}$$

with the quantum numbers $I^G(J^P) = 1^+(1^+)$. For simplicity, here we label the two states $Z_b(10610)$ and $Z_b(10650)$ by Z_b and Z_b', respectively.

Theoretical research had already been performed before the observations of the Z_b states. The authors in Ref. [5, 6] indicated that there may exist a loosely bound S-wave $B\bar{B}^*/B^*\bar{B}$ molecular state.

After the observation, the explanations of the nature of the Z_b states were proposed through different assumptions and theoretical methods. Since the masses of the $Z_b(10610)$ and the $Z_b(10650)$ are close to the $B\bar{B}^*$ and $B^*\bar{B}^*$ thresholds, they are good candidates of $B\bar{B}^*$ and $B^*\bar{B}^*$ molecular states [7–40]. However, tetraquark interpretations including diquark-anti-diquark explanation can not be ruled out [17, 37, 41–47]. As a consequence, in this work we study these two states in the picture of the mixture of molecular and diquark-anti-diquark components, which is used to investigate the nature of the Z_{cs} states observed by LHCb in our previous work [48].

The hadronic molecule has been proposed based on the study of deuteron composed of a proton and a neutron. And this kind of topic has been widely discussed [49–52] within different methods, especially after the observation of $X(3872)$ in 2003 [53]. On the other hand, the concept of the diquark-anti-diquark state was proposed for the first time by Maiani *et al.* [54, 55] following the revitalization of interest on the σ meson. In this work, we use both the molecular state and the diquark-anti-diquark state, and make the calculation in the framework of the effective field theory. In this way, the mesons and the diquarks are viewed as point-like particles, which finally form the color singlet system. The forces between these clusters are provided by exchanging pseudoscalar and vector mesons as well as scalar and axial-vector diquarks.

In order to calculate the effective potentials in the coordinate space, form factors for each vertex are needed, such that the high-momentum contributions are suppressed. In the works related to the One-Boson-Exchange model in the past, the monopole form factor is intro-

*hewei1999@outlook.com
†220220940071@lzu.edu.cn
‡Corresponding Author: sunzf@lzu.edu.cn

Azimuthal Angular Correlation of J/ψ Plus Jet Production at the EIC

Luca Maxia[1, *] and Feng Yuan[2, †]

[1] *Van Swinderen Institute for Particle Physics and Gravity, University of Groningen, Nijenborgh 4, 9747 AG Groningen, The Netherlands*

[2] *Nuclear Science Division, Lawrence Berkeley National Laboratory, Berkeley, CA 94720, USA*

By investigating the soft gluon radiation in the J/ψ plus jet photoproduction at the electron-ion collider (EIC), we demonstrate that the azimuthal angular correlations between the leading jet and heavy quarkonium provide a unique probe to the production mechanism of the latter. In particular, a significant $\cos(\phi)$ asymmetry is found for the color-singlet channel, whereas it vanishes or has an opposite sign for color-octet production, depending on the jet transverse momentum. Numerical results of $\cos(\phi)$ and $\cos(2\phi)$ asymmetries employing both the color-singlet model and the nonrelativistic QCD approach are presented for typical kinematics at the future EIC.

Introduction. In recent years, heavy quarkonium production in various inclusive processes has attracted great interest as a way to probe gluon distributions both in initial (nucleon tomography) and final (fragmentation functions) states [1–17]. Among them, Refs. [10, 12] have studied the azimuthal angular correlation in semi-inclusive DIS between J/ψ and leading jet to probe the so-called linearly polarized gluon distribution. In this paper, we will investigate the dominant contributions from the soft gluon radiations and demonstrate that azimuthal correlations can also provide a unique opportunity to disentangle between the color-singlet (CS) and color-octet (CO) mechanisms.

In the nonrelativistic QCD (NRQCD) [18] approach, the heavy-quark pair forms a Fock state specified by $n = {}^{2S+1}L_J^{[c]}$, with S denoting its spin, L the orbital angular momentum, J the total angular momentum and c its color. Note that, within this framework, the pair can couple either as a CS or CO state. Therefore, comprehending the significance of the CS and CO contributions is crucial. Although great progress has been made in understanding heavy quarkonium production in hadronic collisions (for recent reviews see [19, 20]), challenges remain to phenomenologically describe quarkonium formation and, in particular, to distinguish between these two mechanisms.

In this regard, we will demonstrate how azimuthal angular correlations in J/ψ plus jet photoproduction at the electron-ion collider (EIC) offer a unique probe of the underlying production mechanism. In particular, we will show that these correlations significantly differ between the CS and CO channels. We will focus on the correlation kinematics, i.e., the transverse momentum of individual particles is much larger than the total transverse momentum. Therefore, by combining the transverse momenta of the J/ψ and the jet, $k_{\psi\perp}$ and $k_{j\perp}$ respectively, we can identify two scales. The first one is given by $\vec{P}_\perp = \frac{\vec{k}_{\psi\perp} - \vec{k}_{j\perp}}{2}$, while the second by $\vec{q}_\perp = \vec{k}_{\psi\perp} + \vec{k}_{j\perp}$, with $|\vec{q}_\perp| \ll |\vec{P}_\perp|$. Hence, according to this limit, the heavy quarkonium and jet are mainly produced back-to-back in the transverse plane (see Fig. 1). An imbalance between the two final-state particles with nonzero $|\vec{q}_\perp|$ can be generated by high-order perturbative corrections and from the intrinsic transverse momentum of the incoming parton. We identify this imbalance with the angle ϕ, namely the difference between the azimuthal angles of $\vec{q}_\perp$ and $\vec{k}_{\psi\perp}$, where we can approximate the latter as $\vec{k}_{\psi\perp} \approx \vec{P}_\perp$ within the correlation limit.

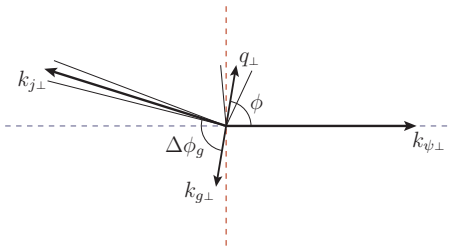

FIG. 1. *Kinematic correlation between the leading jet and heavy quarkonium as viewed in the transverse plane. Here $q_\perp$ (the total outgoing transverse momentum) is small compared to individual transverse momenta.*

Moreover, we remark that in this limit such azimuthal imbalance is mostly generated from the soft/collinear gluon radiation from perturbative diagrams (see for instance Ref. [21, 22]). This contribution, denoted by $k_{g\perp}$ in Fig. 1, tends to align with the jet direction at low $q_\perp$, which leads to significant $\cos(n\phi)$ asymmetries. Detailed examples have been shown for vector boson (photon/Z/Higgs) plus jet production in pp collisions [23, 24] and for lepton plus jet [21] and dijet [22] productions in ep collisions. Nonetheless, this feature is also particularly interesting to investigate the production mechanism of quarkonia.

With this paper, we suggest exploiting azimuthal angular distributions, especially the $\cos(\phi)$ and $\cos(2\phi)$, to unravel the production mechanism. Such findings can

* l.maxia@rug.nl
† fyuan@lbl.gov

Prepared for submission to JHEP

Constraints from the Neutron EDM on Subleading Effective Operators for Direct Dark Matter Searches

Manuel Drees,[a] **Rahul Mehra**[a,1]

[a] *Bethe Center for Theoretical Physics and Physikalisches Institut, Universität Bonn, Nussallee 12, D-53115 Bonn, Germany*

E-mail: drees@th.physik.uni-bonn.de, rmehra@physik.uni-bonn.de

Abstract: Interactions between Dark Matter (DM) and nucleons relevant for direct search experiments can be organised in a model independent manner using a Galiliean invariant, non–relativistic effective field theory (NREFT). Here one expands the interactions in powers of the momentum transfer $\vec{q}$ and DM velocity $\vec{v}$. This approach generates many operators. The potentially most important subleading operators are odd under T, and can thus only be present in a theory with CP violating interactions. We consider two such operators, called $\mathcal{O}_{10}$ and $\mathcal{O}_{11}$ in the literature, in simplified models with neutral spin-0 mediators; the couplings are chosen such that the coefficient of the leading spin independent (SI) operator, which survives for $\vec{v} \to 0$, vanishes at tree level. However, it is generically induced at the next order in perturbation theory. We perform a numerical comparison of the number of scattering events between interactions involving the $T-$odd operators and the corresponding loop induced SI contributions. We find that for "maximal" CP violation the former can dominate over the latter. However, in two of the three models we consider, an electric dipole moment of the neutron (nEDM) is induced at two–loop order. We find that the experimental bound on the nEDM typically leads to undetectably small rates induced by $\mathcal{O}_{10}$. On the other hand, the model leading to a nonvanishing coefficient of $\mathcal{O}_{11}$ does not induce an nEDM.

[1]Corresponding author.

Single charged Higgs pair production in exclusive processes at the LHC

Laura Duarte,[1,*] Victor P. Gonçalves,[1,†] Daniel E. Martins,[2,‡] and Téssio B. de Melo[3,4,§]

[1] *Institute of Physics and Mathematics, Federal University of Pelotas, Postal Code 354, 96010-900, Pelotas, RS, Brazil*

[2] *The Henryk Niewodniczanski Institute of Nuclear Physics (IFJ) Polish Academy of Sciences (PAN), 31-342, Krakow, Poland*

[3] *Universidad Andrés Bello, Facultad de Ciencias Exactas, Departamento de Ciencias Físicas-Center for Theoretical and Experimental Particle Physics, Fernández Concha 700, Santiago, Chile*

[4] *Millennium Institute for Subatomic Physics at the High-Energy Frontier, SAPHIR, Chile*

Abstract

The production of a single charged Higgs boson pair by photon - photon interactions in pp collisions at the LHC is investigated in this exploratory study. We focus on the exclusive production, which is characterized by intact protons and two - rapidity gaps in the final state, and assume the type - I two - Higgs - doublet model, which still allows a light charged Higgs. Assuming the leptonic $H^{\pm} \to [\tau\nu_{\tau}]$ decay mode, we derive predictions for the transverse momentum, rapidity and invariant mass distributions of the $\tau^{+}\tau^{-}$ pair for different values of the charged Higgs mass. The contribution of different background processes are also estimated. Our results indicate that the contribution of the exclusive $H^{+}H^{-}$ production for the $[\tau^{+}\nu_{\tau}][\tau^{-}\nu_{\tau}]$ final state is non - negligible and can, in principle, be used to searching for a light charged Higgs.

PACS numbers:

Keywords:

*Electronic address: l.duarte@unesp.br

†Electronic address: barros@ufpel.edu.br

‡Electronic address: daniel.ernani@ifj.edu.pl

§Electronic address: tessiomelo@institutosaphir.cl

Identify the new state $Y(3872)$ as the P-wave $D\bar{D}^*/\bar{D}D^*$ resonance

Zi-Yang Lin [1, *] Jun-Zhang Wang [2, †] Jian-Bo Cheng [3, ‡] Lu Meng [4, §] and Shi-Lin Zhu [2, ¶]

[1] *School of Physics, Peking University, Beijing 100871, China*
[2] *School of Physics and Center of High Energy Physics, Peking University, Beijing 100871, China*
[3] *College of Science, China University of Petroleum, Qingdao, Shandong 266580, China*
[4] *Institut für Theoretische Physik II, Ruhr-Universität Bochum, D-44780 Bochum, Germany*

The BESIII Collaboration recently observed a new charmonium-like vector state $Y(3872)$ in $e^+e^- \to D\bar{D}$, which should be the first P-wave $D\bar{D}^*/\bar{D}D^*$ molecular resonance. The experimental and theoretical identification of the P-wave dimeson state holds paramount importance in enhancing our comprehension of the non-perturbative QCD and few-body physics. Its existence is firmly established in a unified meson-exchange model which simultaneously depicts the features of the $\chi_{c1}(3872)$, $Z_c(3900)$ and $T_{cc}(3875)$. This scenario can be directly examined in the $e^+e^- \to D\bar{D}^*/\bar{D}D^*$ cross section to see whether a resonance exists at the threshold. The credibility of the investigations is also ensured by the fact that the P-wave interaction dominantly arises from the well-known long-range pion exchange. Additionally, the existence of the P-wave resonance only depends on the interaction strength and is less sensitive to the potential shapes. We extensively calculate all systems up to P-wave with various quantum numbers and predict a dense population of the $D\bar{D}^*/\bar{D}D^*$ and DD^* states, where the S-wave $D\bar{D}^*/\bar{D}D^*$ state with $I^G(J^{PC}) = 0^-(1^{+-})$, P-wave $D\bar{D}^*/\bar{D}D^*$ state with $I^G(J^{PC}) = 0^+(0^{-+})$, and P-wave DD^* state with $I(J^P) = 0(0^-)$ are more likely to be observed in experiments.

Introduction.— Over the past two decades, a significant number of hadrons defying the spectra predicted by quark models have been observed in the heavy flavor sector, which are typically regarded as the exotica within the realm of Quantum Chromodynamics (QCD), see Refs. [1–7] for reviews. Delving into the structure and dynamics associated with these exotic states holds paramount importance in enhancing our comprehension of the non-perturbative features of low-energy QCD. These states also serve as promising examples for studying the general few-body physics.

Among these exotic states, the $\chi_{c1}(3872)$, $Z_c(3900)$, and $T_{cc}(3875)$ stand out as undeniable "star" examples, believed to be the first charmonium-like state [8], the first manifestly exotic charmonium-like state [9, 10], and the first doubly charmed tetraquark state [11, 12] observed in experiments, respectively. It is particularly intriguing that these three states are closely interconnected. The proximity of the former two states to the $D\bar{D}^*/\bar{D}D^*$ threshold and the latter one to the DD^* threshold positions them as strong candidates for corresponding hadronic molecules. Indeed, prior to the observation of $T_{cc}(3875)$, Li *et al.* had predicted a very loosely bound state of DD^* utilizing the one-boson-exchange model (OBE), with parameters established beforehand while investigating the $\chi_{c1}(3872)$ [13, 14].

In the realm of doubly heavy exotic states, such as the $\chi_{c1}(3872)$, $Z_c(3900)$, and $T_{cc}(3875)$, previous studies have predominantly focused on S-wave dimeson states, encompassing bound states, virtual states, or resonances. However, P-wave states near the threshold are of particular interest and arouse the attention in many fields of physics, see the halo nuclei as P-wave resonances in nuclear physics [15] and the P-wave Feshbach resonances in cold atomic physics [16]. Recently, the BESIII Collaboration discovered a new resonance in $e^+e^- \to D\bar{D}$[17]. Apart from the established 1^{--} states $\psi(3770)$, $\psi(4040)$, $\psi(4160)$, $\psi(4230)$, $\psi(4360)$, $\psi(4415)$, $\psi(4660)$, they observed a new resonance with a significance of over 20σ. Its mass and width are fitted to be $3872.5 \pm 14.2 \pm 3.0$ MeV and $179.7 \pm 14.1 \pm 7.0$ MeV, respectively. Hereafter we use $Y(3872)$ to denote this state. It is worth noting that the coupled-channel analysis of data from Belle and BESIII has the potential to generate a bump at this position without introducing new states. However, it appears to be very challenging in accurately depicting the nearby points [18, 19]. The newly observed state, locating exactly at the $D\bar{D}^*$ threshold, turns out a good candidate of the P-wave $D\bar{D}^*$ resonance.

In this work, we aim to identify it as the first P-wave dimeson state in the doubly heavy sector in the meson-exchange model. By relating the $Y(3872)$ to the S-wave states $\chi_{c1}(3872)$, $Z_c(3900)$ and $T_{cc}^+(3985)$, we make a unified description of these states in the one-boson-exchange (OBE) interaction. The resonance poles are obtained by solving the complex scaled Schrödinger equation in momentum space (The details can be found in Ref. [20]).

For the following three reasons, the predictions regarding the existence of the P-wave resonance are highly reliable. Just as the OBE model has provided a high-precision description of nuclear forces [21], meson-exchange models have also achieved notable success in elucidating heavy flavor hadronic molecules [22–30]. In the 1990s, Törnqvist predicted a deuteron-like $D\bar{D}^*$ bound state, which has been confirmed by the observa-

* lzy_15@pku.edu.cn
† wangjzh2022@pku.edu.cn
‡ jbcheng@upc.edu.cn
§ lu.meng@rub.de
¶ zhusl@pku.edu.cn

Heavy neutral lepton search and $\mu \to e\gamma$ constraints in case of type-I seesaw

Stefano Morisi[1,2]

[1] *Dipartimento di Fisica "Ettore Pancini", Università degli studi di Napoli "Federico II", Complesso Univ. Monte S. Angelo, I-80126 Napoli, Italy*
[2] *INFN - Sezione di Napoli, Complesso Univ. Monte S. Angelo, I-80126 Napoli, Italy*

Abstract

Within type-I seesaw mechanism it is possible to have large (order one) light-heavy neutrino mixing even in case of low right-handed neutrino mass scale (of the order of GeV). This implies large lepton flavor violation. As example we consider the process $\mu \to e\gamma$ that can have a branching up to 10^{-8} within type-I seesaw (in contrast with the tiny value 10^{-54} expected). Such an enhancing of lepton flavor violation can be used to constraint the parameter space of long lived particle experiments.

Observation of neutrino oscillation is an evidence that neutrino are massive and that flavor neutrino states do not coincide with the massive one. The unitary lepton mixing matrix U_ν connecting the two basis introduced by Pontecorvo-Maki-Nakagawa-Sakata (PMNS) has been observed esperimentally to be very different from the identity. Indeed one of the three angles parametrizing U is close to be maximal $\sin^2\theta_{23} \sim 0.5$ and one is large $\sin^2\theta_{12} \sim 0.3$ while the third is small but not zero $\sin^2\theta_{13} \sim 0.02$. Lepton mixing suggests that in the Standard Model can be present Lepton Flavor Violation (LFV) phenomena like $\mu \to e\gamma$. Early computation of this process mediated by the three active light neutrinos gives [1, 2] (see [3, 4] for a recent overview)

$$Br(\mu \to e\gamma) \approx \frac{3\alpha_e}{32\pi}\left|U^*_{\nu_{13}}U_{\nu_{23}}\frac{\Delta m^2_{31}}{M^2_W}\right|^2 \sim 10^{-54}\,, \tag{1}$$

that is very far from actual experimental sensitivity that is $7.5\cdot 10^{-13}$ [5].

Improving the performance of weak supervision searches using transfer and meta-learning

Hugues Beauchesne,[a] **Zong-En Chen**[b] **and Cheng-Wei Chiang**[b,a]

[a] *Physics Division, National Center for Theoretical Sciences, Taipei 10617, Taiwan*

[b] *Department of Physics and Center for Theoretical Physics, National Taiwan University, Taipei 10617, Taiwan*

E-mail: beauchesneh@phys.ncts.ntu.edu.tw, r10222045@ntu.edu.tw, chengwei@phys.ntu.edu.tw

Abstract: Weak supervision searches have in principle the advantages of both being able to train on experimental data and being able to learn distinctive signal properties. However, the practical applicability of such searches is limited by the fact that successfully training a neural network via weak supervision can require a large amount of signal. In this work, we seek to create neural networks that can learn from less experimental signal by using transfer and meta-learning. The general idea is to first train a neural network on simulations, thereby learning concepts that can be reused or becoming a more efficient learner. The neural network would then be trained on experimental data and should require less signal because of its previous training. We find that transfer and meta-learning can substantially improve the performance of weak supervision searches.

EUROPEAN ORGANISATION FOR NUCLEAR RESEARCH (CERN)

Submitted to: Eur. Phys. J. C

CERN-EP-2024-063
5th March 2024

Precise test of lepton flavour universality in W-boson decays into muons and electrons in pp collisions at $\sqrt{s} = 13$ TeV with the ATLAS detector

The ATLAS Collaboration

The ratio of branching ratios of the W boson to muons and electrons, $R_W^{\mu/e} = \mathcal{B}(W \to \mu\nu)/\mathcal{B}(W \to e\nu)$, has been measured using 140 fb^{-1} of pp collision data at $\sqrt{s} = 13$ TeV collected with the ATLAS detector at the LHC, probing the universality of lepton couplings. The ratio is obtained from measurements of the $t\bar{t}$ production cross-section in the ee, $e\mu$ and $\mu\mu$ dilepton final states. To reduce systematic uncertainties, it is normalised by the square root of the corresponding ratio $R_Z^{\mu\mu/ee}$ for the Z boson measured in inclusive $Z \to ee$ and $Z \to \mu\mu$ events. By using the precise value of $R_Z^{\mu\mu/ee}$ determined from e^+e^- colliders, the ratio $R_W^{\mu/e}$ is determined to be

$$R_W^{\mu/e} = 0.9995 \pm 0.0022\,(\text{stat}) \pm 0.0036\,(\text{syst}) \pm 0.0014\,(\text{ext})\,.$$

The three uncertainties correspond to data statistics, experimental systematics and the external measurement of $R_Z^{\mu\mu/ee}$, giving a total uncertainty of 0.0045, and confirming the Standard Model assumption of lepton flavour universality in W-boson decays at the 0.5% level.

Contents

1 Introduction

The assumption of lepton flavour universality, i.e. that the couplings of the charged leptons e, μ and τ to the electroweak gauge bosons are independent of the lepton masses, is a key axiom of the Standard Model of particle physics. This assumption has been tested over a wide range of momentum transfers by studying ratios of partial decay widths (or equivalently, ratios of branching ratios) of various particles to electrons, muons and taus. After correction for mass, phase space and radiative effects, these ratios of decays into leptons of generations i and j are proportional to g_i^2/g_j^2, where g_i is the coupling of lepton i ($= e, \mu, \tau$). The equality of these couplings has been tested to the 0.1–0.2% level in decays of τ leptons, π and K mesons (see for example Ref. [1]). More recently, hints of departures from lepton flavour universality at the level of a few standard deviations were seen in the so-called flavour anomalies in b-hadron decays, e.g. in the processes $B \to D^{(*)}\tau\nu$ vs. $B \to D^{(*)}\ell\nu$ (with $\ell = e$ or μ) [2–7], and in the loop-induced process $b \to s\ell\ell$. However, the latest measurement of $b \to s\ell\ell$ in $B \to K^{(*)}\mu^+\mu^-$ vs. $B \to K^{(*)}e^+e^-$ decays from the LHCb collaboration is in agreement with lepton flavour universality [8], and definitive conclusions have yet to be established.

At high momentum transfer, the branching ratios for the leptonic decays of the W boson to e, μ and τ are expected to be equal to very high precision, given the small sizes of the lepton masses compared to the W boson mass. This assumption has been tested in the production of W-boson pairs in e^+e^- collisions at LEP2, in the production of single W bosons at the Tevatron and Large Hadron Collider (LHC), and by exploiting the two W bosons produced in $t\bar{t}$ events at the LHC. The most precise measurement of $R_W^{\mu/e}$, the ratio of branching ratios for $W \to \mu\nu$ and $W \to e\nu$, was performed by the CMS collaboration with $pp \to t\bar{t}$ events at $\sqrt{s} = 13$ TeV, using a global fit to lepton and jet multiplicities, as well as b-tagging and kinematic information, and has a precision of 0.9% [9]. Measurements of $pp \to W$ cross-sections in the $W \to e\nu$ and $W \to \mu\nu$ decay channels from the ATLAS and LHCb experiments [10, 11], and measurements in $e^+e^- \to W^+W^-$ events from the ALEPH, DELPHI, L3 and OPAL experiments at LEP2 [12] also contribute significantly to the combined value of $R_W^{\mu/e} = 1.002 \pm 0.006$ determined by the Particle Data Group [13].

EUROPEAN ORGANISATION FOR NUCLEAR RESEARCH (CERN)

Submitted to: JHEP

CERN-EP-2023-289
5th March 2024

Measurement of t-channel production of single top quarks and antiquarks in pp collisions at 13 TeV using the full ATLAS Run 2 data sample

The ATLAS Collaboration

The production of single top quarks and top antiquarks via the t-channel exchange of a virtual W boson is measured in proton–proton collisions at a centre-of-mass energy of 13 TeV at the LHC using 140 fb^{-1} of ATLAS data. The total cross-sections are determined to be $\sigma(tq) = 137^{+8}_{-8}$ pb and $\sigma(\bar{t}q) = 84^{+6}_{-5}$ pb for top-quark and top-antiquark production, respectively. The combined cross-section is found to be $\sigma(tq + \bar{t}q) = 221^{+13}_{-13}$ pb and the cross-section ratio is $R_t = \sigma(tq)/\sigma(\bar{t}q) = 1.636^{+0.036}_{-0.034}$. The predictions at next-to-next-to-leading-order in quantum chromodynamics are in good agreement with these measurements. The predicted value of R_t using different sets of parton distribution functions is compared with the measured value, demonstrating the potential to further constrain the functions when using this result in global fits. The measured cross-sections are interpreted in an effective field theory approach, setting limits at the 95% confidence level on the strength of a four-quark operator and an operator coupling the third quark generation to the Higgs boson doublet: $-0.37 < C^{3,1}_{Qq}/\Lambda^2 < 0.06$ and $-0.87 < C^{3}_{\phi Q}/\Lambda^2 < 1.42$. The constraint $|V_{tb}| > 0.95$ at the 95% confidence level is derived from the measured value of $\sigma(tq + \bar{t}q)$. In a more general approach, pairs of CKM matrix elements involving top quarks are simultaneously constrained, leading to confidence contours in the corresponding two-dimensional parameter spaces.

Contents

Observation of $\psi(3686) \to 3\phi$

M. Ablikim[1], M. N. Achasov[4,c], P. Adlarson[75], O. Afedulidis[3], X. C. Ai[80], R. Aliberti[35], A. Amoroso[74A,74C], Q. An[71,58,a], Y. Bai[57], O. Bakina[36], I. Balossino[29A], Y. Ban[46,h], H.-R. Bao[63], V. Batozskaya[1,44], K. Begzsuren[32], N. Berger[35], M. Berlowski[44], M. Bertani[28A], D. Bettoni[29A], F. Bianchi[74A,74C], E. Bianco[74A,74C], A. Bortone[74A,74C], I. Boyko[36], R. A. Briere[5], A. Brueggemann[68], H. Cai[76], X. Cai[1,58], A. Calcaterra[28A], G. F. Cao[1,63], N. Cao[1,63], S. A. Cetin[62A], J. F. Chang[1,58], G. R. Che[43], G. Chelkov[36,b], C. Chen[43], C. H. Chen[9], Chao Chen[55], G. Chen[1], H. S. Chen[1,63], H. Y. Chen[20], M. L. Chen[1,58,63], S. J. Chen[42], S. L. Chen[45], S. M. Chen[61], T. Chen[1,63], X. R. Chen[31,63], X. T. Chen[1,63], Y. B. Chen[1,58], Y. Q. Chen[34], Z. J. Chen[25,i], Z. Y. Chen[1,63], S. K. Choi[10A], G. Cibinetto[29A], F. Cossio[74C], J. J. Cui[50], H. L. Dai[1,58], J. P. Dai[78], A. Dbeyssi[18], R. E. de Boer[3], D. Dedovich[36], C. Q. Deng[72], Z. Y. Deng[1], A. Denig[35], I. Denysenko[36], M. Destefanis[74A,74C], F. De Mori[74A,74C], B. Ding[66,1], X. X. Ding[46,h], Y. Ding[34], Y. Ding[40], J. Dong[1,58], L. Y. Dong[1,63], M. Y. Dong[1,58,63], X. Dong[76], M. C. Du[1], S. X. Du[80], Y. Y. Duan[55], Z. H. Duan[42], P. Egorov[36,b], Y. H. Fan[45], J. Fang[1,58], J. Fang[59], S. S. Fang[1,63], W. X. Fang[1], Y. Fang[1], Y. Q. Fang[1,58], R. Farinelli[29A], L. Fava[74B,74C], F. Feldbauer[3], G. Felici[28A], C. Q. Feng[71,58], J. H. Feng[59], Y. T. Feng[71,58], M. Fritsch[3], C. D. Fu[1], J. L. Fu[63], Y. W. Fu[1,63], H. Gao[63], X. B. Gao[41], Y. N. Gao[46,h], Yang Gao[71,58], S. Garbolino[74C], I. Garzia[29A,29B], L. Ge[80], P. T. Ge[76], Z. W. Ge[42], C. Geng[59], E. M. Gersabeck[67], A. Gilman[69], K. Goetzen[13], L. Gong[40], W. X. Gong[1,58], W. Gradl[35], S. Gramigna[29A,29B], M. Greco[74A,74C], M. H. Gu[1,58], Y. T. Gu[15], C. Y. Guan[1,63], A. Q. Guo[31,63], L. B. Guo[41], M. J. Guo[50], R. P. Guo[49], Y. P. Guo[12,g], A. Guskov[36,b], J. Gutierrez[27], K. L. Han[63], T. T. Han[1], F. Hanisch[3], X. Q. Hao[19], F. A. Harris[65], K. K. He[55], K. L. He[1,63], F. H. Heinsius[3], C. H. Heinz[35], Y. K. Heng[1,58,63], C. Herold[60], T. Holtmann[3], P. C. Hong[34], G. Y. Hou[1,63], X. T. Hou[1,63], Y. R. Hou[63], Z. L. Hou[1], B. Y. Hu[59], H. M. Hu[1,63], J. F. Hu[56,j], S. L. Hu[12,g], T. Hu[1,58,63], Y. Hu[1], G. S. Huang[71,58], K. X. Huang[59], L. Q. Huang[31,63], X. T. Huang[50], Y. P. Huang[1], Y. S. Huang[59], T. Hussain[73], F. Hölzken[3], N. Hüsken[35], N. in der Wiesche[68], J. Jackson[27], S. Janchiv[32], J. H. Jeong[10A], Q. Ji[1], Q. P. Ji[19], W. Ji[1,63], X. B. Ji[1,63], X. L. Ji[1,58], Y. Y. Ji[50], X. Q. Jia[50], Z. K. Jia[71,58], D. Jiang[1,63], H. B. Jiang[76], P. C. Jiang[46,h], S. S. Jiang[39], T. J. Jiang[16], X. S. Jiang[1,58,63], Y. Jiang[63], J. B. Jiao[50], J. K. Jiao[34], Z. Jiao[23], S. Jin[42], Y. Jin[66], M. Q. Jing[1,63], X. M. Jing[63], T. Johansson[75], S. Kabana[33], N. Kalantar-Nayestanaki[64], X. L. Kang[9], X. S. Kang[40], M. Kavatsyuk[64], B. C. Ke[80], V. Khachatryan[27], A. Khoukaz[68], R. Kiuchi[1], O. B. Kolcu[62A], B. Kopf[3], M. Kuessner[3], X. Kui[1,63], N. Kumar[26], A. Kupsc[44,75], W. Kühn[37], J. J. Lane[67], P. Larin[18], L. Lavezzi[74A,74C], T. T. Lei[71,58], Z. H. Lei[71,58], M. Lellmann[35], T. Lenz[35], C. Li[47], C. Li[43], C. H. Li[39], Cheng Li[71,58], D. M. Li[80], F. Li[1,58], G. Li[1], H. B. Li[1,63], H. J. Li[19], H. N. Li[56,j], Hui Li[43], J. R. Li[61], J. S. Li[59], K. Li[1], L. J. Li[1,63], L. K. Li[1], Lei Li[48], M. H. Li[43], P. R. Li[38,k,l], Q. M. Li[1,63], Q. X. Li[50], R. Li[17,31], S. X. Li[12], T. Li[50], W. D. Li[1,63], W. G. Li[1,a], X. Li[1,63], X. H. Li[71,58], X. L. Li[50], X. Y. Li[1,63], X. Z. Li[59], Y. G. Li[46,h], Z. J. Li[59], Z. Y. Li[78], C. Liang[42], H. Liang[1,63], H. Liang[71,58], Y. F. Liang[54], Y. T. Liang[31,63], G. R. Liao[14], L. Z. Liao[50], Y. P. Liao[1,63], J. Libby[26], A. Limphirat[60], C. C. Lin[55], D. X. Lin[31,63], T. Lin[1], B. J. Liu[1], B. X. Liu[76], C. Liu[34], C. X. Liu[1], F. Liu[1], F. H. Liu[53], Feng Liu[6], G. M. Liu[56,j], H. Liu[38,k,l], H. B. Liu[15], H. H. Liu[1], H. M. Liu[1,63], Huihui Liu[21], J. B. Liu[71,58], J. Y. Liu[1,63], K. Liu[38,k,l], K. Y. Liu[40], Ke Liu[22], L. Liu[71,58], L. C. Liu[43], Lu Liu[43], M. H. Liu[12,g], P. L. Liu[1], Q. Liu[63], S. B. Liu[71,58], T. Liu[12,g], W. K. Liu[43], W. M. Liu[71,58], X. Liu[38,k,l], X. Liu[39], Y. Liu[80], Y. Liu[38,k,l], Y. B. Liu[43], Z. A. Liu[1,58,63], Z. D. Liu[9], Z. Q. Liu[50], X. C. Lou[1,58,63], F. X. Lu[59], H. J. Lu[23], J. G. Lu[1,58], X. L. Lu[1], Y. Lu[7], Y. P. Lu[1,58], Z. H. Lu[1,63], C. L. Luo[41], J. R. Luo[59], M. X. Luo[79], T. Luo[12,g], X. L. Luo[1,58], X. R. Lyu[63], Y. F. Lyu[43], F. C. Ma[40], H. Ma[78], H. L. Ma[1], J. L. Ma[1,63], L. L. Ma[50], M. M. Ma[1,63], Q. M. Ma[1], R. Q. Ma[1,63], T. Ma[71,58], X. T. Ma[1,63], X. Y. Ma[1,58], Y. Ma[46,h], Y. M. Ma[31], F. E. Maas[18], M. Maggiora[74A,74C], S. Malde[69], Y. J. Mao[46,h], Z. P. Mao[1], S. Marcello[74A,74C], Z. X. Meng[66], J. G. Messchendorp[13,64], G. Mezzadri[29A], H. Miao[1,63], T. J. Min[42], R. E. Mitchell[27], X. H. Mo[1,58,63], B. Moses[27], N. Yu. Muchnoi[4,c], J. Muskalla[35], Y. Nefedov[36], F. Nerling[18,e], L. S. Nie[20], I. B. Nikolaev[4,c], Z. Ning[1,58], S. Nisar[11,m], Q. L. Niu[38,k,l], W. D. Niu[55], Y. Niu [50], S. L. Olsen[63], Q. Ouyang[1,58,63], S. Pacetti[28B,28C], X. Pan[55], Y. Pan[57], A. Pathak[34], P. Patteri[28A], Y. P. Pei[71,58], M. Pelizaeus[3], H. P. Peng[71,58], Y. Y. Peng[38,k,l], K. Peters[13,e], J. L. Ping[41], R. G. Ping[1,63], S. Plura[35], V. Prasad[33], F. Z. Qi[1], H. Qi[71,58], H. R. Qi[61], M. Qi[42], T. Y. Qi[12,g], S. Qian[1,58], W. B. Qian[63], C. F. Qiao[63], X. K. Qiao[80], J. J. Qin[72], L. Q. Qin[14], L. Y. Qin[71,58], X. S. Qin[50], Z. H. Qin[1,58], J. F. Qiu[1], Z. H. Qu[72], C. F. Redmer[35], K. J. Ren[39], A. Rivetti[74C], M. Rolo[74C], G. Rong[1,63], Ch. Rosner[18], S. N. Ruan[43], N. Salone[44], A. Sarantsev[36,d], Y. Schelhaas[35], K. Schoenning[75], M. Scodeggio[29A], K. Y. Shan[12,g], W. Shan[24], X. Y. Shan[71,58], Z. J. Shang[38,k,l], L. G. Shao[1,63], M. Shao[71,58], C. P. Shen[12,g], H. F. Shen[1,8], W. H. Shen[63], X. Y. Shen[1,63], B. A. Shi[63], H. Shi[71,58], H. C. Shi[71,58], J. L. Shi[12,g], J. Y. Shi[1], Q. Q. Shi[55], S. Y. Shi[72], X. Shi[1,58], J. J. Song[19], T. Z. Song[59], W. M. Song[34,1], Y. J. Song[12,g], Y. X. Song[46,h,n], S. Sosio[74A,74C], S. Spataro[74A,74C], F. Stieler[35], Y. J. Su[63], G. B. Sun[76], G. X. Sun[1], H. Sun[63], H. K. Sun[1], J. F. Sun[19], K. Sun[61], L. Sun[76], S. S. Sun[1,63], T. Sun[51,f], W. Y. Sun[34], Y. Sun[9], Y. J. Sun[71,58], Y. Z. Sun[1], Z. Q. Sun[1,63], Z. T. Sun[50], C. J. Tang[54], G. Y. Tang[1], J. Tang[59], M. Tang[71,58], Y. A. Tang[76], L. Y. Tao[72], Q. T. Tao[25,i], M. Tat[69], J. X. Teng[71,58], V. Thoren[75], W. H. Tian[59], Y. Tian[31,63], Z. F. Tian[76], I. Uman[62B], Y. Wan[55], S. J. Wang [50], B. Wang[1], B. L. Wang[63], Bo Wang[71,58], D. Y. Wang[46,h], F. Wang[72], H. J. Wang[38,k,l], J. J. Wang[76], J. P. Wang [50], K. Wang[1,58], L. L. Wang[1], M. Wang[50], N. Y. Wang[63], S. Wang[38,k,l], S. Wang[12,g], T. Wang[12,g], T. J. Wang[43], W. Wang[59], W. Wang[72], W. P. Wang[35,71,o], X. Wang[46,h], X. F. Wang[38,k,l], X. J. Wang[39], X. L. Wang[12,g], X. N. Wang[1], Y. Wang[61], Y. D. Wang[45], Y. F. Wang[1,58,63], Y. L. Wang[19], Y. N. Wang[45], Y. Q. Wang[1], Yaqian Wang[17], Yi Wang[61], Z. Wang[1,58], Z. L. Wang[72], Z. Y. Wang[1,63], Ziyi Wang[63], D. H. Wei[14], F. Weidner[68], S. P. Wen[1], Y. R. Wen[39], U. Wiedner[3], G. Wilkinson[69], M. Wolke[75], L. Wollenberg[3], C. Wu[39], J. F. Wu[1,8], L. H. Wu[1], L. J. Wu[1,63], X. Wu[12,g], X. H. Wu[34], Y. Wu[71,58], Y. H. Wu[55], Y. J. Wu[31], Z. Wu[1,58], L. Xia[71,58], X. M. Xian[39], B. H. Xiang[1,63], T. Xiang[46,h], D. Xiao[38,k,l], G. Y. Xiao[42], S. Y. Xiao[1], Y. L. Xiao[12,g], Z. J. Xiao[41], C. Xie[42], X. H. Xie[46,h], Y. Xie[50], Y. G. Xie[1,58], Y. H. Xie[6], Z. P. Xie[71,58], T. Y. Xing[1,63], C. F. Xu[1,63], C. J. Xu[59], G. F. Xu[1], H. Y. Xu[66,2,p], M. Xu[71,58], Q. J. Xu[16], Q. N. Xu[30], W. Xu[1], W. L. Xu[66], X. P. Xu[55], Y. C. Xu[77], Z. P. Xu[42], Z. S. Xu[63], F. Yan[12,g], L. Yan[12,g], W. B. Yan[71,58], W. C. Yan[80],

[44] *National Centre for Nuclear Research, Warsaw 02-093, Poland*
[45] *North China Electric Power University, Beijing 102206, People's Republic of China*
[46] *Peking University, Beijing 100871, People's Republic of China*
[47] *Qufu Normal University, Qufu 273165, People's Republic of China*
[48] *Renmin University of China, Beijing 100872, People's Republic of China*
[49] *Shandong Normal University, Jinan 250014, People's Republic of China*
[50] *Shandong University, Jinan 250100, People's Republic of China*
[51] *Shanghai Jiao Tong University, Shanghai 200240, People's Republic of China*
[52] *Shanxi Normal University, Linfen 041004, People's Republic of China*
[53] *Shanxi University, Taiyuan 030006, People's Republic of China*
[54] *Sichuan University, Chengdu 610064, People's Republic of China*
[55] *Soochow University, Suzhou 215006, People's Republic of China*
[56] *South China Normal University, Guangzhou 510006, People's Republic of China*
[57] *Southeast University, Nanjing 211100, People's Republic of China*
[58] *State Key Laboratory of Particle Detection and Electronics, Beijing 100049, Hefei 230026, People's Republic of China*
[59] *Sun Yat-Sen University, Guangzhou 510275, People's Republic of China*
[60] *Suranaree University of Technology, University Avenue 111, Nakhon Ratchasima 30000, Thailand*
[61] *Tsinghua University, Beijing 100084, People's Republic of China*
[62] *Turkish Accelerator Center Particle Factory Group, (A)Istinye University, 34010, Istanbul, Turkey; (B)Near East University, Nicosia, North Cyprus, 99138, Mersin 10, Turkey*
[63] *University of Chinese Academy of Sciences, Beijing 100049, People's Republic of China*
[64] *University of Groningen, NL-9747 AA Groningen, The Netherlands*
[65] *University of Hawaii, Honolulu, Hawaii 96822, USA*
[66] *University of Jinan, Jinan 250022, People's Republic of China*
[67] *University of Manchester, Oxford Road, Manchester, M13 9PL, United Kingdom*
[68] *University of Muenster, Wilhelm-Klemm-Strasse 9, 48149 Muenster, Germany*
[69] *University of Oxford, Keble Road, Oxford OX13RH, United Kingdom*
[70] *University of Science and Technology Liaoning, Anshan 114051, People's Republic of China*
[71] *University of Science and Technology of China, Hefei 230026, People's Republic of China*
[72] *University of South China, Hengyang 421001, People's Republic of China*
[73] *University of the Punjab, Lahore-54590, Pakistan*
[74] *University of Turin and INFN, (A)University of Turin, I-10125, Turin, Italy; (B)University of Eastern Piedmont, I-15121, Alessandria, Italy; (C)INFN, I-10125, Turin, Italy*
[75] *Uppsala University, Box 516, SE-75120 Uppsala, Sweden*
[76] *Wuhan University, Wuhan 430072, People's Republic of China*
[77] *Yantai University, Yantai 264005, People's Republic of China*
[78] *Yunnan University, Kunming 650500, People's Republic of China*
[79] *Zhejiang University, Hangzhou 310027, People's Republic of China*
[80] *Zhengzhou University, Zhengzhou 450001, People's Republic of China*

[a] *Deceased*
[b] *Also at the Moscow Institute of Physics and Technology, Moscow 141700, Russia*
[c] *Also at the Novosibirsk State University, Novosibirsk, 630090, Russia*
[d] *Also at the NRC "Kurchatov Institute", PNPI, 188300, Gatchina, Russia*
[e] *Also at Goethe University Frankfurt, 60323 Frankfurt am Main, Germany*
[f] *Also at Key Laboratory for Particle Physics, Astrophysics and Cosmology, Ministry of Education; Shanghai Key Laboratory for Particle Physics and Cosmology; Institute of Nuclear and Particle Physics, Shanghai 200240, People's Republic of China*
[g] *Also at Key Laboratory of Nuclear Physics and Ion-beam Application (MOE) and Institute of Modern Physics, Fudan University, Shanghai 200443, People's Republic of China*
[h] *Also at State Key Laboratory of Nuclear Physics and Technology, Peking University, Beijing 100871, People's Republic of China*
[i] *Also at School of Physics and Electronics, Hunan University, Changsha 410082, China*
[j] *Also at Guangdong Provincial Key Laboratory of Nuclear Science, Institute of Quantum Matter, South China Normal University, Guangzhou 510006, China*
[k] *Also at MOE Frontiers Science Center for Rare Isotopes, Lanzhou University, Lanzhou 730000, People's Republic of China*
[l] *Also at Lanzhou Center for Theoretical Physics, Lanzhou University, Lanzhou 730000, People's Republic of China*
[m] *Also at the Department of Mathematical Sciences, IBA, Karachi 75270, Pakistan*
[n] *Also at Ecole Polytechnique Federale de Lausanne (EPFL), CH-1015 Lausanne, Switzerland*
[o] *Also at Helmholtz Institute Mainz, Staudinger Weg 18, D-55099 Mainz, Germany*
[p] *Also at School of Physics, Beihang University, Beijing 100191 , China*

(Dated: March 5, 2024)

Using $(2.712 \pm 0.014) \times 10^9$ $\psi(3686)$ events collected by the BESIII detector operating at the BEPCII collider, we report the first observation of $\psi(3686) \to 3\phi$ decay with a significance larger

EUROPEAN ORGANIZATION FOR NUCLEAR RESEARCH (CERN)

CERN-EP-2024-049
2024/03/05

CMS-EXO-22-015

Search for new physics with emerging jets in proton-proton collisions at $\sqrt{s} = 13\,\text{TeV}$

The CMS Collaboration*

Abstract

A search for "emerging jets" produced in proton-proton collisions at a center-of-mass energy of 13 TeV is performed using data collected by the CMS experiment corresponding to an integrated luminosity of $138\,\text{fb}^{-1}$. This search examines a hypothetical dark quantum chromodynamics (QCD) sector that couples to the standard model (SM) through a scalar mediator. The scalar mediator decays into an SM quark and a dark sector quark. As the dark sector quark showers and hadronizes, it produces long-lived dark mesons that subsequently decay into SM particles, resulting in a jet, known as an emerging jet, with multiple displaced vertices. This search looks for pair production of the scalar mediator at the LHC, which yields events with two SM jets and two emerging jets at leading order. The results are interpreted using two dark sector models with different flavor structures, and exclude mediator masses up to 1950 (1850) GeV for an unflavored (flavor-aligned) dark QCD model. The unflavored results surpass a previous search for emerging jets by setting the most stringent mediator mass exclusion limits to date, while the flavor-aligned results provide the first direct mediator mass exclusion limits to date.

Submitted to the Journal of High Energy Physics

*See Appendix A for the list of collaboration members

EUROPEAN ORGANIZATION FOR NUCLEAR RESEARCH (CERN)

CERN-EP-2024-005
2024/03/05

CMS-TOP-23-003

Review of top quark mass measurements in CMS

The CMS Collaboration*

Abstract

The top quark mass is one of the most intriguing parameters of the standard model (SM). Its value indicates a Yukawa coupling close to unity, and the resulting strong ties to the Higgs physics make the top quark mass a crucial ingredient for understanding essential aspects of the electroweak sector of the SM. While it is such an important parameter of the SM, its measurement and interpretation in terms of the Lagrangian parameter are challenging. The CMS Collaboration has performed multiple measurements of the top quark mass, addressing these challenges from different angles: highly precise 'direct' measurements, using the top quark decay products, as well as 'indirect' measurements aiming at accurate interpretations in terms of the Lagrangian parameter. Recent mass measurements using Lorentz-boosted top quarks are particularly promising, opening a new avenue of measurements based on top quark decay products contained in a single particle jet, with superior prospects for accurate theoretical interpretations. Moreover, dedicated studies of the dominant uncertainties in the modelling of the signal processes have been performed. This review offers the first comprehensive overview of these measurements performed by the CMS Collaboration using the data collected at centre-of-mass energies of 7, 8, and 13 TeV.

To be submitted to Physics Reports

*See Appendix B for the list of collaboration members

PROCEEDINGS OF SCIENCE

Angular analyses of rare decays at the LHC

Biplab Dey, on behalf of the LHCb collaboration[a,*]

[a] *Eotvos University, Budapest, Hungary*

E-mail: biplab.dey@cern.ch

Loop-suppressed penguin $b \to s$ transitions are sensitive to heavy New Physics particles propagating inside the loops. Thanks to the large sample sizes from the LHC, we are able to perform multidimensional angular analyses that are sensitive to interferences between the Standard Model and New Physics terms. This article surveys the latest results, primarily from LHCb, on $b \to s\mu^+\mu^-$ electroweak and $b \to s\gamma$ radiative penguins.

16th International Conference on Heavy Quarks and Leptons (HQL2023)
28 November-2 December 2023
TIFR, Mumbai, Maharashtra, India

*Speaker

https://pos.sissa.it/

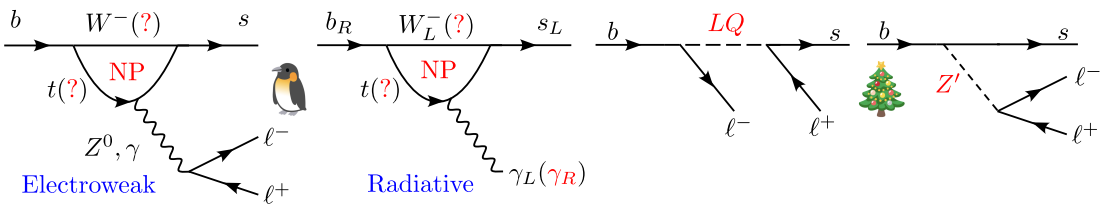

Figure 1: Flavor-changing neutral currents occur only at the loop-level in the SM but can be enhanced by NP effects, both in loop (penguin) and tree-level diagrams.

1. Introduction and theory

In the Standard Model (SM), the flavor-changing neutral current process $b \to s$ is forbidden at the tree-level and proceeds only via loop-suppressed diagrams as shown in Fig. 1. These provide excellent avenues to probe New Physics (NP) contributions that can enter either in loop- or tree-level processes such as via Leptoquarks (LQ) or heavy Z' boson, as shown in Fig. 1. This article focuses on the electroweak (EWP) and radiative (Rad) penguin diagrams, but gluonic penguins can also be an important NP source. A convenient theoretical formalism to study such decays is to regard the SM as a low energy effective field theory containing dimension $d \leq 4$ local operators from renormalizability requirements. Higher dimensional operators can be added with an appropriate cutoff scale Λ, as

$$\mathcal{L}_{\rm eff}(x) = \mathcal{L}_{\rm SM}(x) + \sum_{d>4} \frac{C_i}{\Lambda^{d-4}} \mathcal{O}_i^{(d)}(x) \tag{1}$$

whereby the NP amplitudes have $(E/\Lambda)^{d-4}$ behavior in the energy, E: divergent at high energies, but suppressed at $E \ll \Lambda$. Most relevant for rare $b \to s$ decays are $d = 6$ operators that yield $\mathcal{A}_{\rm eff} \sim C^{\rm SM}/m_W^2 + C^{\rm NP}/\Lambda_{\rm NP}^2$. The basis comprises 10 operators [1]: $O_{1,2}$ (4-quark tree), O_{3-6} (4-quark penguins) and O_8 (gluonic penguin) that are suppressed for the EWP/Rad modes. The dominant left-handed contributions are from the electromagnetic dipole and weak vector (axialvector) operators

$$O_{7\gamma} = \frac{e}{16\pi^2} m_b (\bar{s}\sigma_{\mu\nu} P_R b) F^{\mu\nu}, \quad O_{9V(10A)} = \frac{e^2}{16\pi^2} (\bar{s}\gamma_\mu P_L b)(\bar{\ell}\gamma^\mu(\gamma_5)\ell). \tag{2}$$

The corresponding right-handed (quark side) operators are suppressed in the SM, but can be enhanced in NP scenarios. The dimensionless couplings (Wilson coefficients) associated with the operators in Eq. 2 encode the short distance physics. They are calculated at the m_W scale by integrating out the heavy degrees of freedom from the full theory and evolving to the m_b scale using renormalization group equations. The total amplitudes $\mathcal{A}(i \to f) = C_n(m_b)\langle f|O_n(m_b)|i\rangle_{\rm had}$ also contains the long-distance physics (QCD/hadronization) which mostly comes from *local* form-factors (FFs) that are computed from lattice QCD and other theory tools, but can get important non-local contributions (rescattering, charm loops) that are hard to estimate theoretically.

Thanks to the large $b\bar{b}$ samples available at the LHC, a comprehensive effort on multidimensional angular analyses in $b \to s\ell^+\ell^-$ and $b \to s\vec{\gamma}$ is ongoing. These offer a rich set of angular observables sensitive to $\Delta C_i \equiv C_i^{\rm SM} - C_i^{\rm NP}$. The thrust has been to identify and probe "theoretically clean observables" with reduced dependence on the QCD contributions that often form the

Determination of the resonant parameters of $\chi_{c0}(3915)$ with global fit

Chunhua Li[1,2*] and Xijun Wang[1,2], Chen Wu[1,2]
[1] *Department of physics and electronic technology,*
[2] *Center for Theoretical and Experimental High Energy Physics,*
Liaoning Normal University
Dalian, 116029, P.R.China

The $\chi_{c0}(3915)$ was observed firstly by the Belle experiment in the $\omega J/\psi$ invariant mass spectrum in the process $B \to K\omega J/\psi$, and then confirmed by the Babar experiment. The two experiments reported the resonant parameters of this particle in the both processes $\gamma\gamma \to \omega J/\psi$ and $B \to K\omega J/\psi$ by assuming $\chi_{c0}(3915)$ as a S-wave Breit-Wigner resonance. We perform a global fit to the distributions of invariant mass of $\omega J/\psi$ measured by the Belle and Babar experiments, and incorporate the measurement by the LHCb experiment additionally to extract the mass and width of $\chi_{c0}(3915)$. We obtain $M = 3921.0 \pm 0.9$ MeV/c^2 and $\Gamma = 17.9 \pm 2.2$ MeV which are in good agreement with the values on PDG but with higher precision.

I. INTRODUCTION

Since the first charmonium-like state $X(3872)$ was discovered by Belle experiment via the process $e^+e^- \to \gamma_{ISR}\pi^+\pi^- J/\psi$, a new era of the study of charmonium-like states was triggered [1]. A series of mesons comprised of charmed and anticharmed quark pairs, such as the Y(4260), $X(3915)$, and Zc(3900), were subsequently discovered, and most of them were confirmed by different experiments [2–11]. The understanding of the nature of these particles has turned out to be quite a challenge. Many of them have properties that are quite different from the conventional charmonium, e.g. low open-charm decay rate or absence of hadronic transitions to other charmonium states. To explain these anomalous features, many models have been proposed by theorists, including charmonium molecule mixed states [12, 13], $c\bar{c}g$ hybrid states [15], and tetra-quarks [14]. In addition, the production rates for some of these charmonium-like states are quite low in most experiments which limits the measurement precision of the resonant parameters and the determination of the corresponding quantum numbers, which make the interpretation of these particles difficult. Particle Data Group (PDG) [16] has assigned the $X(3915)$ and $X(3872)$ as the excited spin-triplet charmonium states $\chi_{c0}(2P)$ and $\chi_{c1}(2P)$ named $\chi_{c0}(3915)$ and $\chi_{c1}(3915)$, respectively. We just follow the PDG name convention in the article.

As a member of charmonium-like family of states, the $\chi_{c0}(3915)$ was first observed by the Belle experiment in the process $B \to KJ/\psi\omega$ in a data sample containing 275×10^6 $B\bar{B}$ pairs [9]. The measured mass and width were determined to be $3943 \pm 11 \pm 13$ MeV/c^2 and $87 \pm 22 \pm 26$ MeV with the assumption that the $\chi_{c0}(3915)$ is an S-wave Breit-Wigner (BW) resonance. The particle was confirmed by Babar experiment in the same decy mode with a 383×10^6 $B\bar{B}$ event data sample [10], their reported mass and width were $3914.6^{+3.8}_{-3.4} \pm 2.0$ MeV/c^2 and $34^{+12}_{-8} \pm 5$ MeV. Babar experiment subsequently updated their measurements with a lager data sample of 467×10^6 $B\bar{B}$ events and looser $M(\pi^+\pi^-\pi^0)$ requirements that revealed a X(3872) signal as well [11]; the updated mass and width were $3919.1^{+3.8}_{-3.4} \pm 2.0$ MeV/c^2 and $31^{+10}_{-8} \pm 5$ MeV. In addition, the $\chi_{c0}(3915)$ was also observed in the two-photon collision process $\gamma\gamma \to \omega J/\psi$ by both the Babar and Belle experiments [7, 8]. Their measured masses and widths are listed in Table I. Babar did a spin-parity analysis in their analysis and obtained the quantum number to be $J^P = 0^+$, and identified the $\chi_{c0}(3915)$ as the $\chi_{c0}(2P)$ charmonium state. However, this assignment was disputed because of the large rate for $\chi_{c0}(3915) \to \omega J/\psi$ decay and the absence of $\chi_{c0}(3915) \to D\bar{D}$ decays [17, 18]. Moreover, the mass difference between the $\chi_{c2}(2P)$ and $\chi_{c0}(3915)$ is only about 10 MeV, which is too small for the fine splitting of P-wave charmonia [17]. In 2020, LHCb experiment made an amplitude analysis of the $B^+ \to D^+D^-K^+$ decay [19], and reported that the spin-0 resonance is of necessity to describe the data well and determined its mass and width to be $2923.8 \pm 1.5 \pm 0.4$ MeV/c^2 and $17.4 \pm 5.1 \pm 0.8$ MeV, respectively.

In this article, we perform a simultaneous χ^2 fit to the distributions of invariant mass of $\omega J/\psi$ in the processes of $\gamma\gamma \to \omega J/\psi$ measured by Belle [denoted as (a)], $\gamma\gamma \to \omega J/\psi$ by Babar [(b)], $B^0 \to \omega J/\psi K^0$ by Babar [(c)], $B^+ \to \omega J/\psi K^+$[(d)] by Babar, and $B \to \omega J/\psi K$ by Belle [(e)] to extract the mass and width of $\chi_{c0}(3915)$. The distributions of $M(\omega J/\psi)$ for these processes are shown in Figure 1. Furthermore, LHCb's results are taken into

* chunhua@lnnu.edu.cn

Strangeness plus-one ($S = +1$) resonance-state P_0^{+*} via $K^+n \to K^{*0}p$

Dayoung Lee [1, 2, *] and Seung-il Nam* [1, 2, 3, †]

[1] *Department of Physics, Pukyong National University (PKNU), Busan 48513, Korea*
[2] *Center for Extreme Nuclear Matters (CENuM), Korea University, Seoul 02841, Korea*
[3] *Asia Pacific Center for Theoretical Physics (APCTP), Pohang 37673, Korea*

(Dated: March 5, 2024)

In our current study, we delve into the peak-like structure observed during the reaction process of $K^+n \to K^0p$ at approximately $\sqrt{s} \sim 2.5$ GeV. Our focus centers on exploring the potential $S = +1$ resonance $P_0^{+*} \equiv P_0^*$ as an excited state within the extended vector-meson and baryon (VB) antidecuplet. To achieve this aim, we employ the effective Lagrangian method in conjunction with the (u,t)-channel Regge approach, operating within the tree-level Born approximation. We thoroughly examine various spin-parity quantum numbers for the resonance, resulting in a compelling description of the data, where $M_{P_0^*} \approx 2.5$ GeV and $\Gamma_{P_0^*} \approx 100$ MeV. Furthermore, we propose an experimental technique to amplify the signal-to-noise ratio (S/N) for accurately measuring the resonance. Notably, our findings reveal that background interference diminishes significantly within the K^* forward-scattering region in the center-of-mass frame when the K^* is perpendicularly polarized to the reaction plane. Additionally, we explore the recoil-proton spin asymmetry to definitively determine the spin and parity of the resonance. This study stands to serve as a valuable reference for designing experimental setups aimed at investigating and comprehending exotic phenomena in QCD. Specifically, our insights will inform future J-PARC experiments, particularly those employing higher kaon beam energies.

Keywords: Pentaquark, vector-meson and baryon interaction, $S = +1$ production process, effective Lagrangian method, Regge approach, polarization, resonance, forward-scattering cross-section.

I. INTRODUCTION

Quantum Chromodynamics (QCD) stands as the foundational principle governing the strong interactions among standard-model particles, portraying various hadrons through the non-perturbative interactions of quarks and gluons. It showcases confinement and asymptotic freedom within the framework of non-Abelian color-SU(3) gauge theory. While the minimal composition for baryons is represented by qqq and for mesons by $q\bar{q}$, QCD does not forbid more intricate compositions such as $qqqq\bar{q}$ (pentaquark) and $q\bar{q}q\bar{q}$ (tetraquark), termed *Exotics*. Experimental evidence supporting these exotics has accumulated over decades. The initial observation of the tetraquark meson $X(3872)$, which defies the simple quark model, dates back to 2003, reported by the Belle experiment [1]. Recently, its existence was reaffirmed by the LHCb [2] and CMS [3] experiments, specifying $J^{PS} = 1^{++}$. Additionally, the Belle experiments reported evidence for $Y(4660)$ and $Z(4430)$ in 2007 [4]. Further tetraquark states have been identified via experiments conducted by LHCb, Belle, BES III, Fermilab, and others [5]. Regarding baryons, LHCb reported the $P_c^+(4312, 4440, 4457)$, observed in decay into J/ψ and p [6]. Recently, the same facility detected a novel pentaquark state with the strange-quark s ($udsc\bar{c}$) in the decay of $B^- \to J/\psi\Lambda\bar{p}$ [7]. While not yet definitively confirmed, these pentaquarks can potentially be understood as bound states of vector-meson and baryon (VB), denoted as $P_c^+ \sim D^*\Sigma_c$.

Remarkably, all experimentally observed and confirmed exotics exhibit heavy (charm) flavor. A theoretical rationale for this peculiarity concerning the stability of heavy pentaquarks was elucidated through color-spin interactions among quarks, contrasting with colorless hadronic interactions [8]. While the $S = +1$ light-pentaquark $\Theta^+ \sim uudd\bar{s}$ was reported by the LEPS collaboration [9], supported by the non-topological chiral-quark soliton model [10], its existence remains disputed and unresolved due to varied outcomes across experimental facilities [11]. Furthermore, generating the $S = +1$ resonance dynamically proves challenging within the framework of Weinberg-Tomozawa (WT) type chiral interactions, primarily due to their repulsive nature. Nevertheless, the suggestion of an $S = 0$ pentaquark-like bound-state $P_s^+ \sim uuds\bar{s} \sim K^*\Sigma$, akin to P_c^+ in heavy flavor, was put forth by one of the present authors and collaborators [12, 13], aiming to elucidate the bump structure observed near $\sqrt{s} \approx 2.1$ GeV in $\gamma p \to \phi p$ [14]. In Ref. [14], the existence of P_s^+ was found to be crucial for reproducing the nontrivial structure observed in the spin-density matrix elements (SDMEs), in addition to successfully describing the angular-dependent cross-sections.

*E-mail: ldyoung0421@pukyong.ac.kr
†E-mail: sinam@pknu.ac.kr (corresponding author)

Quantum-number projected generator coordinate method for ^{21}Ne with a chiral two-nucleon-plus-three-nucleon interaction

W. Lin

School of Physics and Astronomy, Sun Yat-sen University, Zhuhai 519082, P.R. China

E. F. Zhou

School of Physics and Astronomy, Sun Yat-sen University, Zhuhai 519082, P.R. China

J. M. Yao*

School of Physics and Astronomy, Sun Yat-sen University, Zhuhai 519082, P.R. China

H. Hergert

Facility for Rare Isotope Beams, Michigan State University,
East Lansing, Michigan 48824-1321, USA. and
Department of Physics & Astronomy, Michigan State University,
East Lansing, Michigan 48824-1321, USA.

Abstract

In this paper, we report a study of the low-lying states of deformed ^{21}Ne within the framework of quantum-number projected generator coordinate method (PGCM), starting from a chiral two-nucleon-plus-three-nucleon (NN+3N) interaction. The wave functions of states are constructed as a linear combination of a set of axially-deformed Hartree-Fock-Bogliubov (HFB) wave functions with different quadrupole deformations. These HFB wave functions are projected onto different angular momenta and the correct neutron and proton numbers for ^{21}Ne. The results of calculations based on the effective Hamiltonians derived by normal-ordering the 3N interaction with respect to three different reference states, including the quantum-number projected HFB wave functions for ^{20}Ne, ^{22}Ne, and an ensemble of them with equal weights, are compared. This study serves as a key step towards ab initio calculations of odd-mass deformed nuclei with the in-medium GCM.

PACS numbers:

*Electronic address: yaojm8@sysu.edu.cn

Prepared for submission to JINST

Abatement of Ionizing Radiation for Superconducting Quantum Devices

B. Loer,[a,1] **P. M. Harrington,**[b] **B. Archambault,**[a] **E. Fuller,**[a] **B. Pierson,**[a] **I. Arnquist,**[a] **K. Harouaka,**[a] **T. D. Schlieder,**[a] **D. K. Kim,**[c] **A. J. Melville,**[c] **B. M. Niedzielski,**[c] **J. L. Yoder,**[c] **K. Serniak,**[b,c] **W. D. Oliver,**[b,c] **J. L. Orrell,**[a] **R. Bunker,**[a] **B. A. VanDevender,**[a] **M. Warner**[a]

[a] *Pacific Northwest National Laboratory, 902 Battelle Boulevard, Richland, WA, USA*

[b] *Research Laboratory of Electronics, Massachusetts Institute of Technology, Cambridge, MA 02139, USA*

[c] *MIT Lincoln Laboratory, 244 Wood Street, Lexington, MA, USA*

E-mail: ben.loer@pnnl.gov

Abstract: Ionizing radiation has been shown to reduce the performance of superconducting quantum circuits. In this report, we evaluate the expected contributions of different sources of ambient radioactivity for typical superconducting qubit experiment platforms. Our assessment of radioactivity inside a typical cryostat highlights the importance of selecting appropriate materials for the experiment components nearest to qubit devices, such as packaging and electrical interconnects. We present a shallow underground facility (30-meter water equivalent) to reduce the flux of cosmic rays and a lead shielded cryostat to abate the naturally occurring radiogenic gamma-ray flux in the laboratory environment. We predict that superconducting qubit devices operated in this facility could experience a reduced rate of correlated multi-qubit errors by a factor of approximately 20 relative to the rate in a typical above-ground, unshielded facility. Finally, we outline overall design improvements that would be required to further reduce the residual ionizing radiation rate, down to the limit of current generation direct detection dark matter experiments.

Keywords: Interaction of radiation with matter; Superconducting devices and qubits; Detector modeling and simulations

[1] Corresponding author.

A Light-Front Model for the Transition Distribution Amplitudes for Backward Timelike Compton Scattering

Barbara Pasquini[1, 2, *] and Andrea Schiavi[b1, ‡]

[1] *Dipartimento di Fisica, Università degli Studi di Pavia, I-27100 Pavia, Italy*
[2] *Istituto Nazionale di Fisica Nucleare, Sezione di Pavia, I-27100 Pavia, Italy*

(Dated: March 4, 2024)

To access information on the internal structure of the nucleon, data from a variety of scattering experiments can be analyzed, in regimes where the information factorizes from an otherwise known scattering amplitude. A recent development, promising new insight, is the study of exclusive reactions in the backward kinematical region, where the information can be encoded in Transition Distribution Amplitudes (TDAs). We model the photon-to-nucleon TDAs, entering the factorized description of backward Timelike Compton Scattering, using techniques of light-front dynamics to integrate information from a quark model for the photon and the nucleon. We include the results of numerical predictions that could inform further experiments at Jefferson Lab and the future Electron–Ion Collider.

I. INTRODUCTION

Hard exclusive processes offer invaluable insight into unraveling the parton structure of hadrons. Notable examples include Deeply-Virtual Compton Scattering (DVCS) and its time-reversal conjugate process, Timelike Compton Scattering (TCS). The former is the scattering of a high-virtuality spacelike photon off a nucleon target, resulting in the production of a real photon and the recoiling nucleon, while the latter sees a real photon scatter off the nucleon target into a high-virtuality timelike photon. In the forward kinematical region, characterized by small absolute values of the Mandelstam variable t and large absolute values of the Mandelstam variable u, information on the internal structure of the nucleon is encoded in Generalized Parton Distributions (GPDs) [1–11]. These are related to matrix elements of a bilocal operator between the initial and final nucleon states, and represent the amplitude of transferring momentum to the hadron through the exchange of two partons.

The situation is more complex in the backward kinematical region, where $|u|$ is small and $|t|$ is large. However, the analogy with forward DVCS and TCS suggests a description in terms of a soft amplitude factorized from the hard scattering of the partons with the probe. The variable u characterizes the transition between a real photon and a nucleon, which can be encoded in Transition Distribution Amplitudes (TDAs) [12, 13]. These are related to matrix elements of a trilocal operator between the photon and nucleon states, and represent the amplitude of transferring momentum and one unit of baryon number through the exchange of three partons.

The focus of the present work is on backward TCS, which remains relatively unexplored compared to other processes involving TDAs [14–18]. The experimental study of TCS is a recent development, with data published for the first time in 2021 by the CLAS collaboration at Jefferson Lab for the forward region [19]. Moreover, backward TCS is expecially appealing, since the electromagnetic Bethe–Heitler background, where the initial photon directly couples to a lepton–antilepton pair in the final state, is significantly suppressed (except for very narrow regions of solid angle for the produced lepton) [13]. To compare the factorized description against experimental results and to guide further phenomenological studies, a model for the photon-to-nucleon TDAs is required, beginning with the leading contributions.

The model developed in this work is based on the framework of light-front dynamics (LFD) [20–23], where the interacting particles are described in the Fock space in terms of light-front wave functions (LFWFs). In Sec. II, the backward kinematical region of TCS is analyzed, and the factorized description of the scattering amplitude is introduced. The photon-to-nucleon TDAs are defined, and their expressions in terms of matrix elements of a trilocal operator between the initial photon and the final nucleon states are derived. Section III is dedicated to modelling the photon-to-nucleon TDAs, specifically in the support region where the description in terms of the leading Fock-components of the photon and nucleon LFWFs is suitable. The photon is treated as a light quark–antiquark pair, while the Fock representation of the nucleon is truncated to the three valence quarks in a constituent quark model that has already been applied to GPDs [24–29] and to nucleon-to-neutral-pion TDAs [18]. Given the impracticality of

[b] Currently employed in high-school teaching.
[*] Electronic address: barbara.pasquini@unipv.it
[‡] Electronic address: andrearschiavi@gmail.com

Five-dimensional collective Hamiltonian with improved inertial functions

Kouhei Washiyama,[1,2,*] Nobuo Hinohara,[1,3] and Takashi Nakatsukasa[1,3,4]

[1] *Center for Computational Sciences, University of Tsukuba, Tsukuba 305-8577, Japan*
[2] *Research Center for Superheavy Elements, Kyushu University, Fukuoka 819-0395, Japan*
[3] *Faculty of Pure and Applied Sciences, University of Tsukuba, Tsukuba 305-8571, Japan*
[4] *RIKEN Nishina Center, Wako 351-0198, Japan*

(Dated: March 4, 2024)

Background: To describe shape fluctuations associated with large-amplitude collective motion in the quadrupole degrees of freedom, the five-dimensional collective Hamiltonian (5DCH) has been widely used. The inertial functions in the 5DCH are microscopically calculated with the energy density functional (EDF) theory employing the cranking formula. However, since the cranking formula ignores dynamical residual effects, it is known to fail to reproduce the correct inertial functions, for instance, the total mass for the translational motion.

Purpose: We aim to resolve problems of the insufficient description of the inertial functions in the 5DCH. We provide a practical method to include the dynamical residual effects in the inertial functions that depend on the quadrupole deformation parameters β and γ.

Methods: We use the local quasiparticle random-phase approximation (LQRPA) based on the constrained Hartree-Fock-Bogoliubov states in the β–γ plane with the Skyrme EDF. The finite-amplitude method is used for efficient computations of the LQRPA.

Results: The inertial functions evaluated with the LQRPA significantly increase from the ones with the cranking formula due to the dynamical residual effects. This increase also shows a strong β–γ dependence. We show an application of the present method to a transitional nucleus ^{110}Pd. The low-lying positive-parity spectra are well reproduced with the LQRPA inertial functions.

Conclusions: We clarify the importance of the dynamical residual effects in the inertial functions of the 5DCH for the description of the low-lying spectra. The 5DCH with the improved inertial functions provides a reliable and efficient description of low-lying spectra in nuclei associated with the quadrupole shape fluctuation.

Introduction. A proper and feasible description of the shape dynamics in the ground and the excited states is one of the important subjects in nuclear physics. Observations of spectroscopic properties in nuclei suggest the existence of shape fluctuations and shape coexistence phenomena in low-lying states in nuclei, particularly in the so-called transitional regions from spherical to deformed shapes in the nuclear chart [1].

The self-consistent nuclear energy density functional (EDF) theory has often been employed to describe ground-state properties of nuclei [2, 3]. To describe shape fluctuations and shape coexistence phenomena associated with large-amplitude collective motion, it is necessary to use beyond-mean-field methods. The generator-coordinate method (GCM) with the quadrupole deformation parameters β and γ as generator coordinates [4–9] has been developed and shown the importance of including the triaxial degree of freedom, γ. Recently, the standard GCM was extended to construct the basis states stochastically [10, 11] and variationally [12]. Although the GCM is a fully quantum theory, in practice, we need to combine the GCM with the projection method to recover the broken symmetries. The GCM with the projection method requires a large amount of numerical computations. In addition, there remain many unsolved issues with realistic EDFs [3]. For instance, the discontinuities and divergences are caused by the fractional powers of the density dependence in EDFs [13, 14].

As an alternative approach to the GCM, the five-dimensional collective Hamiltonian (5DCH) method [15, 16] with the intrinsic quadrupole deformation parameters (β, γ) and the three Euler angles has been extensively used based on the EDF [16–20]. In most of the EDF-based 5DCH studies, the inertial functions in the vibrational and rotational kinetic energies are calculated according to the formula in the adiabatic perturbation [21], which is identical to the well-known Inglis-Belyaev (IB) formula for the rotational moment of inertia [22, 23]. The vibrational masses are further approximated by the so-called perturbative cranking formula [24]. The cranking formula ignores variation of the self-consistent potential induced by the collective motion, known as the dynamical residual effects, thus, giving an insufficient description of the inertial functions [25]. In particular, the absence of the time-odd terms of the dynamical mean field leads to the violation of the Galilean symmetry and is known to produce the wrong translational mass [26]. Despite such drawbacks, the cranking formula has been widely used [16–20], because the full inclusion of the dynamical residual effects in the inertial functions requires a huge computational cost. Some recent 5DCH studies [20, 27] evaluate the rotational moments of inertia within the cranked Hartree-Fock-Bogoliubov (HFB) framework that are equivalent to the Thouless-Valatin inertia [28] to include the dynamical residual effects in the rotational kinetic energy. In many of the former studies, a phe-

* E-mail: washiyama@nucl.ph.tsukuba.ac.jp

Electroproduction of the Λ/Σ^0 hyperons at $Q^2 \simeq 0.5$ $(\mathrm{GeV}/c)^2$ in forward angles

K. Okuyama,[1] K. Itabashi,[2] S. Nagao,[3] S.N. Nakamura,[1,3] K.N. Suzuki,[4] T. Gogami,[4] B. Pandey,[5,6] L. Tang,[5,7] P. Bydžovský,[8] D. Skoupil,[8] T. Mart,[9] D. Abrams,[10] T. Akiyama,[1] D. Androic,[11] K. Aniol,[12] C. Ayerbe Gayoso,[13] J. Bane,[14] S. Barcus,[13] J. Barrow,[14] V. Bellini,[15] H. Bhatt,[16] D. Bhetuwal,[16] D. Biswas,[5] A. Camsonne,[7] J. Castellanos,[17] J-P. Chen,[7] J. Chen,[13] S. Covrig,[7] D. Chrisman,[18,19] R. Cruz-Torres,[20] R. Das,[21] E. Fuchey,[21] K. Gnanvo,[10] F. Garibaldi,[15,22] T. Gautam,[5] J. Gomez,[7] P. Gueye,[5,19] T.J. Hague,[23] O. Hansen,[7] W. Henry,[7] F. Hauenstein,[24] D.W. Higinbotham,[7] C.E. Hyde,[24] M. Kaneta,[1] C. Keppel,[7] T. Kutz,[21] N. Lashley-Colthirst,[5] S. Li,[25,26] H. Liu,[27] J. Mammei,[28] P. Markowitz,[17] R.E. McClellan,[7] F. Meddi,[15,29] D. Meekins,[7] R. Michaels,[7] M. Mihovilovic,[30,31,32] A. Moyer,[33] D. Nguyen,[20,34] M. Nycz,[23] V. Owen,[13] C. Palatchi,[10] S. Park,[21] T. Petkovic,[11] S. Prematilake,[10] P.E. Reimer,[35] J. Reinhold,[17] S. Riordan,[35] V. Rodriguez,[36] C. Samanta,[6] S.N. Santiesteban,[25] B. Sawatzky,[7] S. Širca,[30,31] K. Slifer,[25] T. Su,[23] Y. Tian,[37] Y. Toyama,[1] K. Uehara,[1] G.M. Urciuoli,[15] D. Votaw,[18,19] J. Williamson,[38] B. Wojtsekhowski,[7] S.A. Wood,[7] B. Yale,[25] Z. Ye,[35] J. Zhang,[10] and Z. Zhang[10]

(JLab Hypernuclear Collaboration)

[1] *Department of Physics, Graduate School of Science, Tohoku University, Sendai, Miyagi 980-8578 Japan*
[2] *WPI-QUP, KEK, Oho 1-1, Tsukuba, Ibaraki 305-0801,Japan*
[3] *Department of Physics, Graduate School of Science, The University of Tokyo, Hongo, Tokyo 113-0033 Japan*
[4] *Department of Physics, Graduate School of Science, Kyoto University, Kyoto, Kyoto 606-8502 Japan*
[5] *Department of Physics, Hampton University, Hampton, Virginia 23668, USA*
[6] *Department of Physics & Astronomy, Virginia Military Institute, Lexington, Virginia 24450, USA*
[7] *Thomas Jefferson National Accelerator Facility, Newport News, Virginia 23606, USA*
[8] *Nuclear Physics Institute, ASCR, 25068 Řež/Prague, Czech Republic*
[9] *Departemen Fisika, FMIPA, Universitas Indonesia, Depok 16424, Indonesia*
[10] *Department of Physics, University of Virginia, Charlottesville, Virginia 22904, USA*
[11] *Department of Physics & Department of Applied Physics, University of Zagreb, HR-10000 Zagreb, Croatia*
[12] *Physics and Astronomy Department, California State University, Los Angeles, California 90032, USA*
[13] *Department of Physics, The College of William and Mary, Virginia 23185, USA*
[14] *Department of Physics, University of Tennessee, Knoxville, Tennessee 37996, USA*
[15] *Istituto Nazionale di Fisica Nucleare, Sezione di Roma, 00185, Rome, Italy*
[16] *Department of Physics, Mississippi State University, Mississippi State, Mississippi 39762, USA*
[17] *Department of Physics, Florida International University, Miami, Florida 33199, USA*
[18] *Department of Physics and Astronomy, Michigan State University, East Lansing, Michigan 48824, USA*
[19] *National Superconducting Cyclotron Laboratory, Michigan State University, East Lansing, MI 48824, USA*
[20] *Department of Physics, Massachusetts Institute of Technology, Cambridge, Massachusetts 02139, USA*
[21] *Department of Physics, State University of New York, Stony Brook, New York 11794, USA*
[22] *Instituto Superiore di Sanità, 00161, Rome, Italy*
[23] *Department of Physics, Kent State University, Kent, Ohio 44242 USA*
[24] *Department of Physics, Old Dominion University, Norfolk, Virginia 23529, USA*
[25] *Department of Physics, University of New Hampshire, Durham, New Hampshire 03824, USA*
[26] *Nuclear Science Division, Lawrence Berkeley National Laboratory, Berkeley, CA 94720, USA*
[27] *Department of Physics, Columbia University, New York, New York 10027, USA*
[28] *Department of Physics and Astronomy, University of Manitoba, Winnipeg, Manitoba R3T 2N2, Canada*
[29] *Sapienza University of Rome, I-00185, Rome, Italy*
[30] *Faculty of Mathematics and Physics, University of Ljubljana, 1000 Ljubljana, Slovenia*
[31] *Jožef Stefan Institute, Ljubljana, Slovenia*
[32] *Institut für Kernphysik, Johannes Gutenberg-Universität Mainz, DE-55128 Mainz, Germany*
[33] *Department of Physics, Christopher Newport University, Newport News, Virginia 23606, USA*
[34] *University of Education, Hue University, Hue City, Vietnam*
[35] *Physics Division, Argonne National Laboratory, Lemont, Illinois 60439, USA*
[36] *División de Ciencias y Tecnologia, Universidad Ana G. Méndez, Recinto de Cupey, San Juan 00926, Puerto Rico*
[37] *Department of Physics, Syracuse University, New York, New York 10016, USA*
[38] *School of Physics & Astronomy, University of Glasgow, Glasgow, G12 8QQ, Scotland, UK*

In 2018, the E12-17-003 experiment was conducted at the Thomas Jefferson National Accelerator Facility (JLab) to explore the possible existence of an $nn\Lambda$ state in the reconstructed missing mass distribution from a tritium gas target. As part of this investigation, data was also collected using a gaseous hydrogen target, not only for a precise absolute mass scale calibration but also for the study of Λ/Σ^0 electroproduction. This dataset was acquired at $Q^2 \simeq 0.5$ $(\mathrm{GeV}/c)^2$, $W = 2.14$ GeV, and $\theta_{\gamma \mathrm{K}}^{\mathrm{c.m.}} \simeq 8$ deg. It covers forward angles where photoproduction data is scarce and a low-Q^2 region that is of interest for hypernuclear experiments. On the other hand, this kinematic region is at a slightly higher Q^2 than previous hypernuclear experiments, thus providing crucial information for understanding the Q^2 dependence of the differential cross sections for Λ/Σ^0 hyperon electroproduction. This paper reports on the Q^2 dependence of the differential cross section for the $e + p \to e' + K^+ + \Lambda/\Sigma^0$ reaction in the $0.2 - 0.8$ $(\mathrm{GeV}/c)^2$, and provides comparisons with the currently available theoretical models.

I. INTRODUCTION

Studying the production of hyperons and hypernuclei provides invaluable insights into baryon-baryon interactions with an extended flavor, strangeness. Due to the short lifetime of the Λ hyperon/hypernucleus ($\sim 10^{-10}$ s), it cannot be observed as a stable state naturally. However, one can consider a Λ-hypernucleus as a stable object in view of the strong interaction. The development of accelerator facilities and detection techniques has made it possible to produce and study hyperons and hypernuclei in laboratories.

The study of hyperons and hypernuclei systems via the $(e, e'K^+)$ reaction at the Thomas Jefferson National Accelerator Facility (JLab) has been one its cornerstone program since the mid 90s. Understanding (un)polarized differential cross section for hyperon electroproduction is a fundamental observable to estimate the production yield of hypernuclei. However, experimental data on hyperon electroproduction under various kinematic settings is far from satisfactory. Therefore, predictions from theoretical models have become vital to supplement the data, in particular, at low-Q^2 and forward angles.

Isobaric models, based on effective Lagrangian using hadron degrees of freedom, play an important role: Kaon-Maid [1, 2], Saclay-Lyon A [3, 4], and other [5–9] models describe kaon-hyperon production with reasonable agreement compared to the existing experimental data.

In these isobaric models, background contribution from t-channel and/or u-channel often becomes problematic when describing the kaon-hyperon channel. As a countermeasure, Regge-plus-resonance (RPR) models, which introduces Regge pole exchange, have been recently applied to strangeness electroproduction with good results [10–12].

In the One-Photon-Exchange-Approximation (OPEA), the electroproduction process $p(e, e'K^+)\Lambda/\Sigma^0$ can be related to the photoproduction one via a virtual photon $p(\gamma^*, K^+)\Lambda/\Sigma^0$ as shown in Fig. 1. This relation is given by [13],

$$\frac{\mathrm{d}^3\sigma}{\mathrm{d}E_{\mathrm{e}'}\mathrm{d}\Omega_{\mathrm{e}'}\mathrm{d}\Omega_{\mathrm{K}}^{\mathrm{c.m.}}} = \Gamma \frac{\mathrm{d}\sigma_{\gamma^*}}{\mathrm{d}\Omega_{\mathrm{K}}^{\mathrm{c.m.}}}, \tag{1}$$

where Γ is the so-called virtual photon flux. $\mathrm{d}\sigma_{\gamma^*}/\mathrm{d}\Omega_{\mathrm{K}}^{\mathrm{c.m.}}$ is regarded as a differential cross section for the kaon-hyperon production from a virtual photon. The four-momentum of a virtual photon is denoted as $q^\mu := (\omega/c, \boldsymbol{q}) = (E_{\mathrm{e}}/c - E_{\mathrm{e}'}/c, \boldsymbol{P}_{\mathrm{e}} - \boldsymbol{P}_{\mathrm{e}'})$. The difference between photoproduction and electroproduction can be related using the four-momentum transfer, $Q^2 := -q^2 = -\omega^2/c^2 + |\boldsymbol{q}|^2$, i.e., $Q^2 = 0$ for photoproduction and $Q^2 > 0$ for electroproduction.

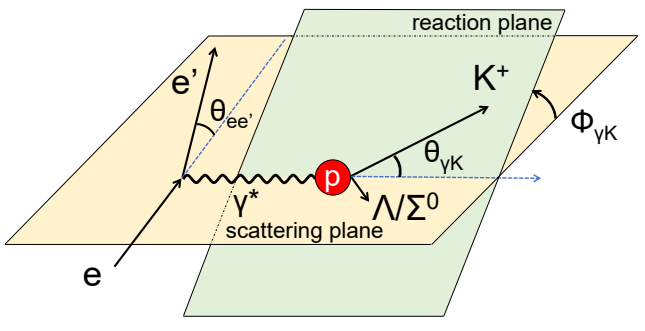

FIG. 1. Schematic drawing of the $p(e, e'K^+)\Lambda/\Sigma^0$ reaction. This shows the $\Lambda/\Sigma^0 - K^+$ production under One-Photon-Exchange-Approximation.

The differential cross section for virtual photoproduction can be decomposed into 4 terms when polarization observables are not measured in either the initial or the final state as in the present experiment,

$$\frac{\mathrm{d}\sigma_{\gamma^*}}{\mathrm{d}\Omega_{\mathrm{K}}^{\mathrm{c.m.}}} = \frac{\mathrm{d}\sigma_{\mathrm{T}}}{\mathrm{d}\Omega_{\mathrm{K}}^{\mathrm{c.m.}}} + \varepsilon \frac{\mathrm{d}\sigma_{\mathrm{TT}}}{\mathrm{d}\Omega_{\mathrm{K}}^{\mathrm{c.m.}}} \cos 2\phi_{\gamma \mathrm{K}} + \varepsilon \frac{\mathrm{d}\sigma_{\mathrm{L}}}{\mathrm{d}\Omega_{\mathrm{K}}^{\mathrm{c.m.}}} + \sqrt{2\varepsilon\,(\varepsilon + 1)} \frac{\mathrm{d}\sigma_{\mathrm{LT}}}{\mathrm{d}\Omega_{\mathrm{K}}^{\mathrm{c.m.}}} \cos \phi_{\gamma \mathrm{K}}. \tag{2}$$

Each term can be calculated using theoretical models and subsequently combined as in Eq. (2) to obtain $\mathrm{d}\sigma_{\gamma^*}/\mathrm{d}\Omega_{\mathrm{K}}^{\mathrm{c.m.}}$. In section V, comparison of our experimental results to theoretical calculations will be discussed.

Hyperon electroproduction has been performed primarily at JLab, while hyperon photoproduction experiments have been performed by CLAS at JLab [14–17], SAPHIR at ELSA [18], LEPS at SPring-8 [19], and GRAAL at ESRF [20]. Experimentally, the photoproduction process has been well investigated providing abundant data for a wide range of angles to test theoretical models. However, there are still large amounts of disagreements among the models due to the lack of data on photoproduction at forward and backward angles. The electroproduction process has the advantage of

universe

MDPI

Review

Recent Findings from Heavy-Flavor Angular Correlation Measurements in Hadronic Collisions

Deepa Thomas [1,*] and Fabio Colamaria [2,*]

[1] The University of Texas at Austin, Department of Physics, 2515 Speedway, Austin, TX 78712, USA
[2] Istituto Nazionale di Fisica Nucleare, Sezione di Bari, Via E. Orabona, 4 - 70125 Bari, Italy
* Correspondence: deepa.thomas@utexas.edu (D.T.); fabio.colamaria@ba.infn.it (F.C.)

Abstract: The study of angular correlations of heavy-flavor particles in hadronic collisions can provide crucial insight into the heavy quark production, showering, and hadronization processes. The comparison with model predictions allows us to discriminate among different approaches for heavy quark production and hadronization, as well as different treatments of the underlying event employed by the models to reproduce correlation observables. In ultra-relativistic heavy-ion collisions, where a deconfined state of matter, the quark–gluon plasma (QGP), is created, heavy-flavor correlations can shed light on the modification of the heavy quark fragmentation due to the interaction between charm and beauty quarks with the QGP constituents, as well as characterize their energy loss processes while traversing the medium. Insight into the possible emergence of collective-like mechanisms in smaller systems, resembling those observed in heavy-ion collisions, can also be obtained by performing correlation studies in high-multiplicity proton–proton and proton–nucleus collisions. In this review, the most recent and relevant measurements of heavy-flavor correlations performed in all collision systems at the LHC and RHIC will be presented, and the new understandings that they provide will be discussed.

Keywords: heavy quarks; correlations; jet fragmentation; energy loss; collectivity in small systems; heavy quark production; hadronization

Citation: Thomas, D.; Colamaria, F. Recent Findings from Heavy-Flavor Angular Correlation Measurements in Hadronic Collisions. *Universe* **2024**, *10*, 0. https://doi.org/

Academic Editor: Firstname Lastname

Received: 15 January 2024
Revised: 6 February 2024
Accepted: 7 February 2024
Published:

1. Introduction

The study of heavy quark (charm and beauty quarks) production in high-energy hadronic collisions is an important tool to test and validate perturbative quantum chromodynamics (pQCD) calculations [1–4], as they are produced in hard parton scattering processes. The production cross-section of several heavy-flavor hadrons and their decay products has been measured at different centers of mass energies at RHIC [5–7], Tevatron [8–10], and at the LHC [11–32], and are compared with pQCD calculations [3,33–37]. The correlated production of heavy flavors, studied as a function of variables such as the azimuthal angle between heavy-flavor particles, either by direct reconstruction of heavy-flavor hadrons or from their decay products, can provide a significantly larger amount of information than single-particle inclusive heavy-flavor production.

In ultra-relativistic heavy-ion collisions, heavy quarks play an important role in the study of the deconfined phase of strongly interacting matter, the quark–gluon plasma (QGP), created in these collisions. Traditional observables of heavy quarks, such as the nuclear modification factor (R_{AA}) and the elliptic flow coefficient (v_2), have been extensively studied at RHIC [38–40] and at the LHC [12,41–44]. These measurements indicate that heavy quarks experience significant in-medium energy loss at large transverse momentum (p_T), and that charm quarks partially thermalize within the medium at smaller p_T. These effects are induced by the interaction of heavy quarks with the medium constituents, mainly made up of light partons. The interaction has two main contributions, the purely elastic process, resulting in a collisional energy loss [45–47], and gluon bremsstrahlung, producing